

# UC Berkeley

## SEMM Reports Series

### Title

A New Dissipative Time-Stepping Algorithm for Frictional Contact Problems: Formulation and Analysis

### Permalink

<https://escholarship.org/uc/item/2sg4m3z0>

### Authors

Armero, Francisco


Petocz, Eva

### Publication Date

1997-08-01

REPORT NO.  
UCB/SEMM-97/13

STRUCTURAL ENGINEERING  
MECHANICS AND MATERIALS



A NEW DISSIPATIVE  
TIME-STEPPING ALGORITHM FOR  
FRICTIONAL CONTACT PROBLEMS:  
FORMULATION AND ANALYSIS

BY

F. ARMERO

AND

E. PETOCZ

AUGUST 1997

DEPARTMENT OF CIVIL AND ENVIRONMENTAL ENGINEERING  
UNIVERSITY OF CALIFORNIA, BERKELEY

# A New Dissipative Time-Stepping Algorithm for Frictional Contact Problems: Formulation and Analysis.

by

F. ARMERO and E. PETŐCZ

Structural Engineering, Mechanics and Materials  
Department of Civil and Environmental Engineering  
University of California, Berkeley CA 94720

## Abstract

This paper presents a new time-stepping algorithm for frictional contact problems that exhibits unconditional positive energy dissipation. More specifically, the proposed scheme preserves a-priori stability estimates of the continuum problem for both frictionless and frictional contact, leading to improved numerical stability properties in particular. For the normal contact component, the algorithm exhibits full energy conservation between released states, while the energy does not increase over its initial value due to the enforcement of the normal contact constraint during persistent contact. A penalty regularization is considered to this purpose. A new regularization of the stick conditions is considered for the frictional part. The new scheme is shown rigorously to exhibit positive energy dissipation like the continuum physical problem in this frictional case. Coulomb friction is assumed. Complete analyses of these considerations, as well as a detailed description of their finite element implementation, are included in the general finite deformation range. Representative numerical simulations are presented to assess the performance of the newly proposed methods.

## 1. Introduction

The numerical analysis and simulation of contact problems is probably one of the most difficult and demanding tasks in typical practical applications of computational solid mechanics. The cause of this inherent difficulty can be traced to the unilaterally constrained character of the impenetrability constraint between solids. The introduction of frictional effects adds on these difficulties with the need to model non-smooth stick/slip conditions. As a consequence, the resulting problems are numerically stiff, highly non-smooth, and strongly nonlinear. Explicit integration schemes are popular nowadays to avoid some of these difficulties. Explicit methods, however, are known to be only conditionally stable in time. In fact, the stability restriction becomes a severe limitation in usual applications involving contact, due again to the very stiff nature of constrained problems.

The improved stability properties of implicit schemes are often needed for efficient analyses of problems that do not require the resolution of short time scales. However, standard implicit schemes are known to exhibit instabilities in nonlinear problems. In fact, time-stepping algorithms that are unconditionally stable, or even dissipative, for linear problems may become unstable in a nonlinear setting. See e.g. the numerical examples in SIMO & TARNOW [1992] and the results presented herein, where such instabilities are observed even in the physically dissipative context of frictional contact problems. Given these considerations, the goal of the research presented in this paper can be stated as the development of implicit time-stepping algorithms for contact problems that possess unconditional (energy) stability in time and lead to a stable enforcement of the contact constraints. Dynamic contact/impact problems are of particular interest. More specifically, we require that the numerical algorithm inherits a-priori stability estimates of the continuum problem. In this context, we develop in this paper a time-stepping algorithm for frictional contact problems that is rigorously shown to be energy dissipative, as the physical system.

The analysis and numerical simulation of contact problems has been the subject of intensive research in the past. Early efforts in the area of dynamic contact problems can be found in HUGHES et al [1976], HALLQUIST et al [1985], and BATHE & CHAUDHARY [1985], among others; see also the comprehensive account in KIKUCHI & ODEN [1988]. The formulations presented in BELYTSCHKO & NEAL [1991], CARPENTER et al [1991], and MUNJIZA et al [1995] are some examples of more recent works focusing on the enforcement of the contact constraints in the context of explicit integrators for dynamic contact problems. But more recently, we can find a special interest in the formulation of improved implicit schemes for dynamic contact problems. The recent works of TAYLOR & PAPADOPOULOS [1993], LEE [1994], and LAURSEN & CHAWLA [1996] are representative examples, with an emphasis on frictionless contact. See also the results presented in ARMERO & PETŐCZ [1996], and described below. These efforts can be considered as part of the current interest in the development of more robust time-stepping algorithms for nonlinear elastodynamics. In this context, the formulation of energy-momentum conserving schemes for nonlinear elastic systems (as presented in SIMO & TARNOW [1992], CRISFIELD & SHI [1994], and GONZALEZ & SIMO [1995], among others) is of special significance for the work presented herein.

We have presented recently in ARMERO & PETŐCZ [1996] a new class of conserving time-stepping algorithms for frictionless contact. The proposed schemes are based on a penalty regularization of the normal contact constraint, and inherit the conservation properties of the continuum problem. More specifically, the energy of the system of solids does not increase due to the imposition of the contact constraint (part is stored in the penalty regularization potential), and it is fully restored upon release. Extensions imposing the associated constraints in the velocity have been presented also. Altogether, the newly proposed schemes have not only shown a superior stability properties in time but also

an improved enforcement of the contact constraint when compared with more traditional implicit schemes. In fact, we have observed that traditional mid-point and trapezoidal rules, and even the dissipative HHT method, are prone to numerical instabilities in the context of frictionless contact, often leading to the actual blow-up of the numerical computation, in contrast with the proposed conserving schemes. The reader is referred to the aforementioned reference for further details.

In the present paper, we consider the general case of frictional contact, in the continuum framework described in LAURSEN & SIMO [1993]. More specifically, we present a new time-stepping algorithm for frictional contact that leads to positive energy dissipation. A crucial ingredient of the new scheme is the integration of the friction law based on a properly defined (numerical) slip function. This definition arises from a second order approximation of the evolution equations defining the contact kinematics. This new slip function is employed in the integration of the constrained equations modeling the stick/slip conditions. Furthermore, a new penalty regularization of the stick condition is considered, having a similar structure to classical elastoplasticity. Coulomb friction is assumed for the evolution of the frictional slip. The resulting discrete evolution equations are shown rigorously to lead to a decrease of the energy of the solids (i.e., positive energy dissipation), in compliance with the dissipative nature of the frictional problem. The fully nonlinear range involving finite kinematics is assumed in these developments. In fact, invariance issues are carefully considered. As a consequence, the newly proposed schemes are not only frame indifferent, but the resulting discrete contact contributions exhibit the conservation properties of linear and angular momentum characteristic of their continuum counterparts. The newly proposed scheme applies to both dynamic and quasi-static problems. We develop in detail the finite element implementation of these methods.

An outline of the rest of the paper is as follows. Section 2 summarizes the continuum formulation of the frictional contact between solids. In particular, Section 2.3 describes in detail the conservation laws of linear and angular momenta characteristic of a free system of solids in contact, frictionless or frictional, as well as the energy conservation/dissipation in the continuum problem. A-priori stability estimates to be inherited by the numerical algorithms are derived in this section. We develop in Section 3 the newly proposed time-stepping algorithms. In particular, Section 3.3 presents the proof of the dissipative properties of the new schemes. We assess the performance of the proposed methods in Section 4 with several representative numerical simulations. Both quasi-static and dynamic problems are presented. Finally, Section 5 concludes with some final remarks.

## 2. The Governing Equations

We describe in this section the notation and the governing equations describing the contact of solids, as employed in the rest of the paper. Section 2.1 describes the kinematics

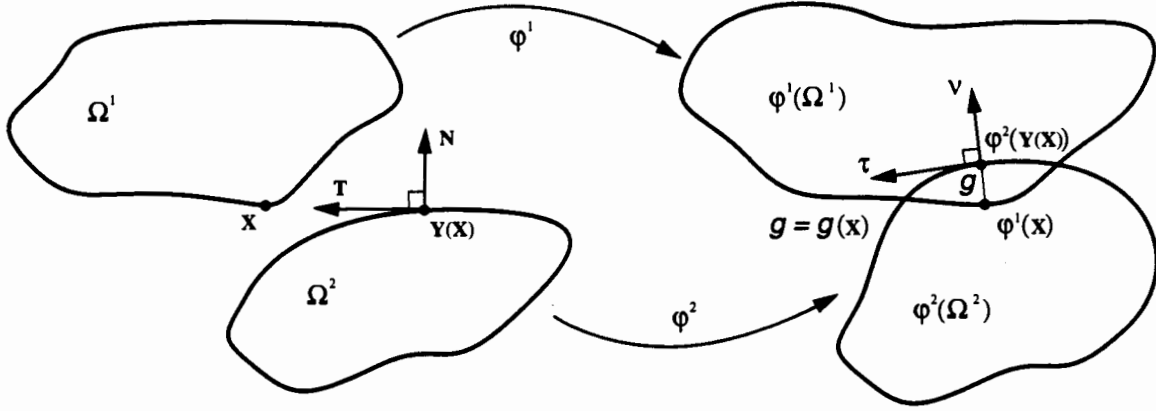


**FIGURE 2.1.** Frictional contact between two solids. Definition of the gap function  $g(\mathbf{X})$ , closest-point projection  $\mathbf{Y}(\mathbf{X})$ , unit normal  $\boldsymbol{\nu}$ , reference tangent bases  $\mathbf{T}$  and  $\boldsymbol{\tau}$ , for the two dimensional case.

of contact. The fully nonlinear finite deformation range is assumed. Section 2.2 summarizes the weak form of the governing equations as required for the development of the finite element methods proposed herein. Further details of the material summarized in these sections can be found in WRIGGERS et al [1990] and LAURSEN & SIMO [1993]. Section 2.3 summarizes the conservation laws that arise in the the contact of solids. In particular, we describe in detail the evolution of the energy and identify the dissipative character of the frictional problem. These developments define the a-priori stability estimates to be preserved by the numerical methods developed in Section 3.

## 2.1. The kinematics of contact

Let the domains  $\Omega^{(i)} \subset \mathbb{R}^{n_{\text{dim}}}$  ( $n_{\text{dim}} = 1, 2$  or  $3$ ) with smooth boundaries  $\Gamma^{(i)} = \partial\Omega^{(i)}$  represent the reference placement of  $n_{\text{body}}$  solid bodies ( $i = 1, n_{\text{body}}$ ). Without loss of generality, we shall present the following developments for the particular case of two solids,  $n_{\text{body}} = 2$ . We refer to the material particles by  $\mathbf{X} \in \Omega^{(i)}$ , and let  $\boldsymbol{\varphi}^{(i)} : \Omega^{(i)} \times [0, T] \rightarrow \mathbb{R}^{n_{\text{dim}}}$  be the deformations of each solid to a current placement  $\boldsymbol{\varphi}_t^{(i)}(\Omega^{(i)})$  (with  $\boldsymbol{\varphi}_t^{(i)}(\mathbf{X}) \equiv \boldsymbol{\varphi}^{(i)}(\mathbf{X}, t)$ ) at a certain instant  $t \in [0, T]$  for a time interval  $T$ . Let  $\gamma_{c,t}^{(i)} \subset \boldsymbol{\varphi}^{(i)}(\partial\Omega^{(i)})$  denote two parts of the boundaries of the respective solids in contact, as defined below. The subscript  $t$  emphasizes the dependence of these boundary segments on the time  $t$ . We denote the corresponding material boundaries by  $\Gamma_{c,t}^{(i)} := \boldsymbol{\varphi}^{(i)-1}(\gamma_{c,t}^{(i)})$ .

In this context, we define the closest-point projection mapping  $\hat{\mathbf{Y}}(t) : \Gamma_{c,t}^{(1)} \rightarrow \Gamma_{c,t}^{(2)}$  at the time  $t$  as

$$\hat{\mathbf{Y}}(\mathbf{X}, t) = \arg \min_{\mathbf{Y} \in \Gamma^{(2)}} \|\boldsymbol{\varphi}_t^{(1)}(\mathbf{X}) - \boldsymbol{\varphi}_t^{(2)}(\mathbf{Y})\|, \quad (2.1)$$

for  $\mathbf{X} \in \Gamma_{c,t}^{(1)}$  and Euclidean norm  $\|\cdot\|$  in  $\mathbb{R}^{n_{\text{dim}}}$ . Given the definition (2.1), a standard

argument shows the orthogonality property

$$\llbracket \boldsymbol{\varphi}_t \rrbracket := \boldsymbol{\varphi}_t^{(1)}(\mathbf{X}) - \boldsymbol{\varphi}_t^{(2)}(\hat{\mathbf{Y}}(\mathbf{X}, t)) = g \boldsymbol{\nu} , \quad (2.2)$$

for the unit normal  $\boldsymbol{\nu}$  to  $\gamma_{c,t}^{(2)}$  at  $\boldsymbol{\varphi}_t^{(2)}(\hat{\mathbf{Y}}(\mathbf{X}, t))$ . To simplify the notation we do not write a subscript  $t$  indicating the dependence on time of the geometric quantities  $g$ ,  $\boldsymbol{\nu}$ , and others introduced below. Figure 2.1 sketches the construction behind the closes-point projection (2.1) in the two dimensional case.

Expression (2.2) defines also the gap function  $g$ , as

$$g = \hat{g}(\mathbf{X}, t) = \llbracket \boldsymbol{\varphi}_t \rrbracket \cdot \boldsymbol{\nu} , \quad (2.3)$$

which is imposed to satisfy the unilateral contact constraint

$$g \geq 0 , \quad (2.4)$$

at all times  $t$ . In this context, the contact boundary  $\Gamma_{c,t}^{(1)}$  is defined by

$$\Gamma_{c,t}^{(1)} = \{ \mathbf{X} \in \Gamma^{(1)} : g(\mathbf{X}, t) \geq 0 \} , \quad (2.5)$$

and the boundary  $\Gamma_{c,t}^{(2)}$  as the image of  $\Gamma_{c,t}^{(1)}$  under the closest-point projection  $\mathbf{Y} = \hat{\mathbf{Y}}(\mathbf{X}, t)$ . Since in this continuum setting we impose the constraint (2.4), we conclude that

$$\gamma_{c,t}^{(1)} \equiv \gamma_{c,t}^{(1)} \equiv \cap_{i=1}^2 \partial \left( \boldsymbol{\varphi}_t^{(i)}(\Omega^{(i)}) \right) , \quad (2.6)$$

with no special role played by the ordering of the solids. The numerical schemes described in Section 3 consider a penalty regularization of the unilateral constraint (2.4), leading to an approximate satisfaction of the constraint (2.4). In this context, one refers to the surface  $\Gamma^{(1)}$  as the slave surface which is required not to penetrate the master surface  $\Gamma^{(2)}$ , as it was introduced in HALLQUIST et al [1985]. Double passes schemes avoiding the special role assigned to each surface by a particular ordering of the solids are also discussed in this reference.

Following LAURSEN & SIMO [1993], we introduce the following notation. Let the vectors  $\{\mathbf{T}_\alpha\}$  ( $\alpha = 1, n_{\text{dim}} - 1$ ) define a basis of the tangent space to  $\Gamma_{c,t}^{(2)}$ , not orthonormal in general. See Figure 2.1 for an illustration of the reference basis  $\mathbf{T} \equiv \mathbf{T}_1$  in the two dimensional case. We denote by

$$M_{\alpha\beta} := \mathbf{T}_\alpha \cdot \mathbf{T}_\beta , \quad (2.7)$$

the associated metric, a positive definite matrix. We consider the spatial vectors

$$\boldsymbol{\tau}_\alpha := \mathbf{F}^{(2)} \mathbf{T}_\alpha = \boldsymbol{\varphi}_{,\alpha}^{(2)} , \quad (2.8)$$

defining a convected basis  $\{\boldsymbol{\tau}_\alpha\}$  of the tangent space to  $\gamma_{c,t}^{(2)}$ . The standard notation

$$\mathbf{F}^{(i)} := \text{Grad}\boldsymbol{\varphi}^{(i)} \quad i = 1, 2, \quad (2.9)$$

is used for the deformation gradients. We denote the associated metric by

$$m_{\alpha\beta} := \boldsymbol{\tau}_\alpha \cdot \boldsymbol{\tau}_\beta, \quad (2.10)$$

and the corresponding dual basis by

$$\boldsymbol{\tau}^\alpha := m^{\alpha\beta} \boldsymbol{\tau}_\beta \quad \alpha = 1, n_{\text{dim}} - 1, \quad (2.11)$$

with  $[m^{\alpha\beta}] = [m_{\alpha\beta}]^{-1}$ . Summation over repeated Greek indices is assumed hereafter, e.g., addition on  $\beta = 1, n_{\text{dim}} - 1$  is implied in (2.11). The orthogonality relations

$$\boldsymbol{\tau}_\alpha \cdot \boldsymbol{\nu} = \boldsymbol{\tau}^\alpha \cdot \boldsymbol{\nu} = 0, \quad (2.12)$$

follow from the previous definitions.

Crucial to the development of the numerical schemes proposed in Section 3 is the evaluation of the change of the closest-point projection constraint (2.2) in time. To calculate this time derivative, we consider the rate of the closest-point  $\mathbf{Y} = \hat{\mathbf{Y}}(\mathbf{X}, t)$  given by

$$\dot{\mathbf{Y}} = \dot{\xi}^\alpha \mathbf{T}_\alpha, \quad (2.13)$$

defining the values  $\dot{\xi}^\alpha$  in terms of the tangent basis  $\{\mathbf{T}_\alpha\}$  in the reference configuration. The vector field  $\dot{\mathbf{Y}}$  defines a relative slip velocity.

The material time derivative of (2.2) reads

$$[[\mathbf{V}]] - \mathbf{F}^{(2)} \dot{\mathbf{Y}} = \dot{g}\boldsymbol{\nu} - g \left[ \mathbf{V}_{,\alpha}^{(2)} + \boldsymbol{\tau}_{\alpha,\beta} \dot{\xi}^\beta \right] \cdot \boldsymbol{\tau}^\alpha, \quad (2.14)$$

in terms of the jump of the material velocities

$$[[\mathbf{V}]] = \mathbf{V}^{(1)}(\mathbf{X}, t) - \mathbf{V}^{(2)}(\hat{\mathbf{Y}}(\mathbf{X}, t), t), \quad (2.15)$$

at a particular time  $t$ , with

$$\mathbf{V}^{(i)} := \dot{\boldsymbol{\varphi}}_t^{(i)} := \frac{d\boldsymbol{\varphi}_t^{(i)}}{dt} \quad i = 1, 2. \quad (2.16)$$

We note that the second fundamental form of the surface  $\gamma_{c,t}^{(2)}$  is given by  $b_{\alpha\beta} = -\boldsymbol{\tau}_{\alpha,\beta} \cdot \boldsymbol{\nu}$ , and it is symmetric. Combining (2.8) and (2.13) with the orthogonality relations (2.12), the normal component of equation (2.14) can be written as

$$\boxed{\dot{g} = [[\mathbf{V}]] \cdot \boldsymbol{\nu}}, \quad (2.17)$$



and the tangential components as

$$\boxed{A_{\alpha\beta}\dot{\xi}^\beta = [\mathbf{V}] \cdot \boldsymbol{\tau}_\alpha + g \mathbf{V}_{,\alpha}^{(2)} \cdot \boldsymbol{\nu} ,} \quad (2.18)$$

in terms of the symmetric matrix

$$A_{\alpha\beta} := m_{\alpha\beta} + g b_{\alpha\beta} , \quad (2.19)$$

assumed invertible at all times. Hence, equation (2.18) defines the slip rates  $\dot{\xi}^\beta$  uniquely in terms of the material velocities of each solid. For the limit contact problem ( $g = 0$ ), the invertibility of  $A_{\alpha,\beta}$  follows readily from the positive definiteness of the spatial metric  $m_{\alpha\beta}$ . Since the case of interest involves the enforcement of the contact constraint (2.4), and therefore it is close to this limit case, this assumption is not excessively restrictive.

## 2.2. The weak form of the governing equations

The evolution of the system of solids described in the previous section is governed by the balance of linear momentum, given in weak form by the variational relation (see WRIGGERS et al [1990] and LAURSEN & SIMO [1993])

$$\begin{aligned} \sum_{i=1}^2 \left\{ \int_{\Omega^{(i)}} \left[ \rho_o^{(i)} \dot{\mathbf{V}}^{(i)} \cdot \delta \boldsymbol{\varphi}^{(i)} + \mathbf{S}^{(i)} : \mathbf{F}^{(i)T} \text{Grad}(\delta \boldsymbol{\varphi}^{(i)}) \right] d\Omega^{(i)} \right. \\ \left. - \int_{\Omega^{(i)}} \rho_o^{(i)} \mathbf{b}^{(i)} \cdot \delta \boldsymbol{\varphi}^{(i)} d\Omega^{(i)} - \int_{\Gamma_{T,t}^{(i)}} \bar{\mathbf{t}}^{(i)} \cdot \delta \boldsymbol{\varphi}^{(i)} d\Gamma^{(i)} \right\} \\ + \int_{\Gamma_{c,t}^{(1)}} [-p\delta g + t_{T\alpha} \delta \xi^\alpha] d\Gamma^{(1)} = 0 , \end{aligned} \quad (2.20)$$

for all admissible variations  $\delta \boldsymbol{\varphi}^{(i)} \in \mathcal{V}^{(i)}$  ( $i = 1, 2$ ), with

$$\mathcal{V}^{(i)} = \{ \boldsymbol{\eta} : \Omega^{(i)} \rightarrow \mathbb{R}^{n_{\text{dim}}} : \boldsymbol{\eta} = 0 \text{ on } \Gamma_u^{(i)} \} , \quad (2.21)$$

that is, variations satisfying the homogeneous essential boundary conditions as usual. In this way, the deformations  $\boldsymbol{\varphi}^{(i)}$  are assumed to satisfy the essential boundary conditions

$$\boldsymbol{\varphi}_t^{(i)} = \bar{\boldsymbol{\varphi}}_t^{(i)} \quad \text{on } \Gamma_{u,t}^{(i)} \quad (i = 1, 2) , \quad (2.22)$$

for given boundary functions  $\bar{\boldsymbol{\varphi}}_t^{(i)}$ . In (2.20), we have used the notation  $\rho_o^{(i)}$  for the reference density of solid ( $i$ ),  $\dot{\mathbf{V}}^{(i)}$  for the material acceleration,  $\mathbf{S}^{(i)}$  for the second Piola-Kirchhoff stress tensor, and body forces  $\mathbf{b}^{(i)}$  and nominal applied tractions  $\bar{\mathbf{t}}^{(i)}$  on  $\Gamma_{T,t}^{(i)} \subset \Gamma^{(i)}$  ( $i = 1, 2$ ). The conditions

$$\Gamma_{u,t}^{(i)} \cap \Gamma_{T,t}^{(i)} \cap \Gamma_{c,t}^{(i)} = \emptyset \quad \text{and} \quad \overline{\Gamma_{u,t}^{(i)} \cup \Gamma_{T,t}^{(i)} \cup \Gamma_{c,t}^{(i)}} = \Gamma^{(i)} \quad i = 1, 2 , \quad (2.23)$$

are assumed for each time  $t$  for a well-posed problem. The symmetry of the second Piola-Kirchhoff

$$\mathbf{S}^{(i)} = \mathbf{S}^{(i)T} \quad \forall i = 1, 2, \quad (2.24)$$

follows from material frame indifference. The general dynamic case has been assumed in (2.20), hence requiring the specification of initial conditions

$$\boldsymbol{\varphi}_{t=0}^{(i)} = \boldsymbol{\varphi}_o^{(i)}, \quad \text{and} \quad \boldsymbol{\varphi}_{t=0}^{(i)} = \mathbf{V}_o \quad (i = 1, 2), \quad (2.25)$$

for given initial deformations and velocities, respectively. The quasi-static problem is recovered by assuming a vanishing density in the transient term as it is common practice.

The variations of the gap and slip in the contact contribution, last term of (2.20), are given in terms of the variations  $\delta\boldsymbol{\varphi}^{(i)}$  by

$$\delta g = \llbracket \delta\boldsymbol{\varphi} \rrbracket \cdot \boldsymbol{\nu}, \quad (2.26)$$

and

$$A_{\alpha\beta} \delta\xi^\beta = \llbracket \delta\boldsymbol{\varphi} \rrbracket \cdot \boldsymbol{\tau}_\alpha + g \delta\boldsymbol{\varphi}_{,\alpha}^{(2)} \cdot \boldsymbol{\nu}, \quad (2.27)$$

respectively, by taking the variation of (2.2), which proceeds exactly as the derivation of (2.17) and (2.18). As noted below, the expressions (2.26) and (2.27) lead to an invariant form of the contact forces with respect to translations and rotation, leading to the conservation of linear and angular momenta as described in the following section.

In (2.20), the nominal contact traction  $\mathbf{t}^{(1)}$  on  $\Gamma_{c,t}^{(1)}$  has been decomposed in a normal and tangential component as

$$\mathbf{t}^{(1)} = p \boldsymbol{\nu} - \mathbf{t}_T, \quad \text{where} \quad \mathbf{t}_T := t_{T\alpha} \boldsymbol{\tau}^\alpha. \quad (2.28)$$

The nominal pressure  $p$  is the Lagrange multiplier enforcing the unilateral constraint (2.4), and satisfies the Kuhn-Tucker complimentary conditions

$$p \geq 0, \quad g \geq 0, \quad \text{and} \quad pg = 0. \quad (2.29)$$

The consistency condition

$$p\dot{g} = 0, \quad (2.30)$$

follows, and defines the case of persistent contact.

The evolution of the tangential traction  $\mathbf{t}_T$  is governed by the friction law. Frictional slip occurs when a certain level of the tangential tractions is reached. We consider herein the classical Coulomb law given by the slip relation

$$\mathbf{v} = \gamma \frac{\mathbf{t}_T}{\|\mathbf{t}_T\|}. \quad (2.31)$$

As proposed in LAURSEN & SIMO [1993], an invariant expression of the slip velocity  $\mathbf{v}$  in (2.31) is obtained as

$$\mathbf{v} := M_{\alpha\beta} \dot{\xi}^\beta \boldsymbol{\tau}^\alpha . \quad (2.32)$$

Alternative definitions are discussed in Remark 2.1 of Section 2.3 below. The consistency parameter  $\gamma$  in (2.31) is determined by the stick/slip conditions

$$\phi := \|\mathbf{t}_T\| - \mu p \leq 0 , \quad (2.33)$$

$$\gamma \geq 0 , \quad \gamma \phi = 0 , \quad \text{and} \quad \gamma \dot{\phi} = 0 , \quad (2.34)$$

where the Euclidean norm  $\|\cdot\|$  in  $\mathbb{R}^{n_{\text{dim}}}$  is given by

$$\|\mathbf{t}_T\|^2 = m^{\alpha\beta} t_{T\alpha} t_{T\beta} , \quad (2.35)$$

in the convected surface basis. A constant friction coefficient  $\mu \geq 0$  is assumed in (2.33) for simplicity. This concludes the definition of the problem of interest. We describe next the conservation/dissipation properties of the final governing equations.

### 2.3. The conservation laws and energy dissipation

The system of equations (2.20) possesses a number of conservation laws in the presence of symmetries of the problem. For instance, under the assumption of a free system of solids, that is,

$$\mathbf{b}^{(i)} = 0 , \quad \bar{\mathbf{t}}^{(i)} = 0 , \quad \text{and} \quad \Gamma_{u,t}^{(i)} = \emptyset \quad i = 1, 2 , \quad (2.36)$$

the total linear and angular momenta are conserved. We summarize in this section these conservation laws together with the evolution of the total energy of the system of solids.

**i. Linear momentum.** Define the total linear momentum by

$$\mathbf{L} := \sum_{i=1}^2 \int_{\Omega^{(i)}} \rho^{(i)} \mathbf{V}^{(i)} d\Omega^{(i)} . \quad (2.37)$$

Under the assumption (2.36)<sub>3</sub>, an admissible set of variations is obtained by

$$\boldsymbol{\varphi}^{(i)} = \mathbf{a} \in \mathcal{V}^{(i)} \quad i = 1, 2 , \quad (2.38)$$

for a constant vector  $\mathbf{a} \in \mathbb{R}^{n_{\text{dim}}}$ . By noting that the gap variation  $\delta g$  and slip variations  $\delta \xi^\beta$ , defined respectively by (2.26) and (2.27), vanish

$$\frac{d\mathbf{L}}{dt} \cdot \mathbf{a} = \int_{\Omega^{(i)}} \rho^{(i)} \dot{\mathbf{V}}^{(i)} \cdot \mathbf{a} d\Omega^{(i)} = 0 \quad \forall \mathbf{a} \in \mathbb{R}^{n_{\text{dim}}} , \quad (2.39)$$

after inserting the variations (2.38) in the weak equation (2.20). The conservation of linear momentum

$$\mathbf{L} = \text{constant} , \quad (2.40)$$

follows then as a consequence of the invariance of the governing equations under the variations (2.38) (translations).

ii. *Angular momentum.* Define the total angular momentum by

$$\mathbf{J} := \sum_{i=1}^2 \int_{\Omega^{(i)}} \boldsymbol{\varphi}^{(i)} \times \rho^{(i)} \mathbf{V}^{(i)} d\Omega^{(i)} , \quad (2.41)$$

where  $\times$  denotes the cross product of two vectors in  $\mathbb{R}^3$  (and the corresponding embedding in  $\mathbb{R}^{n_{\text{dim}}}$  if  $n_{\text{dim}} < 3$ ). Under the assumption (2.36)<sub>3</sub>, an admissible set of variations is obtained as

$$\delta\boldsymbol{\varphi}^{(i)} = \mathbf{w} \times \boldsymbol{\varphi}_t^{(i)} \in \mathcal{V}^{(i)} \quad \forall i = 1, 2 , \quad (2.42)$$

for a constant vector  $\mathbf{w} \in \mathbb{R}^{n_{\text{dim}}}$ . In this case, we have

$$\text{Grad} \left( \delta\boldsymbol{\varphi}^{(i)} \right) = \mathbf{F}^{(i)-T} \nabla \left( \delta\boldsymbol{\varphi}^{(i)} \right) = \mathbf{F}^{(i)-T} \widehat{\mathbf{W}} , \quad (2.43)$$

for the spatial gradient  $\nabla(\cdot)$ , and the skew-symmetric matrix  $\widehat{\mathbf{W}}$  with axial vector  $\mathbf{w}$ , that is,

$$\widehat{\mathbf{W}} \mathbf{a} = \mathbf{w} \times \mathbf{a} \quad \forall \mathbf{a} \in \mathbb{R}^{n_{\text{dim}}} . \quad (2.44)$$

The gap variation (2.26) vanishes for the variations (2.42), since

$$\delta g = \left( \mathbf{w} \times \llbracket \boldsymbol{\varphi}_t \rrbracket \right) \cdot \boldsymbol{\nu} = \left( \mathbf{w} \times g \boldsymbol{\nu} \right) \cdot \boldsymbol{\nu} = 0 , \quad (2.45)$$

after using (2.2). Similarly, the slip variations (2.27) vanish for the variations (2.42), since

$$\begin{aligned} A_{\alpha\beta} \delta\xi^\beta &= \left( \mathbf{w} \times \llbracket \boldsymbol{\varphi}_t \rrbracket \right) \cdot \boldsymbol{\tau}_\alpha + g \cdot \left( \mathbf{w} \times \boldsymbol{\varphi}_{,\alpha}^{(2)} \right) \cdot \boldsymbol{\nu} \\ &= \left( \mathbf{w} \times g \boldsymbol{\nu} \right) \cdot \boldsymbol{\tau}_\alpha + g \left( \mathbf{w} \times \boldsymbol{\tau}_\alpha \right) \cdot \boldsymbol{\nu} = 0 , \end{aligned} \quad (2.46)$$

after employing the expression (2.8). Therefore, we obtain the relation

$$\begin{aligned} \frac{d\mathbf{J}}{dt} \cdot \mathbf{w} &= \sum_{i=1}^2 \int_{\Omega^{(i)}} \rho^{(i)} \dot{\mathbf{V}}^{(i)} \cdot \left( \mathbf{w} \times \boldsymbol{\varphi}^{(i)} \right) d\Omega^{(i)} \\ &= - \sum_{i=1}^2 \int_{\Omega^{(i)}} \mathbf{S}^{(i)} : \widehat{\mathbf{W}} d\Omega^{(i)} = 0 \quad \forall \mathbf{w} \in \mathbb{R}^{n_{\text{dim}}} , \end{aligned} \quad (2.47)$$

using the weak equation (2.20) for the free system of solids (2.36). The last equality in (2.47) follows from the symmetry and skew-symmetry of  $\mathbf{S}^{(i)}$  and  $\widehat{\mathbf{W}}$ , respectively. The conservation of angular momentum

$$\mathbf{J} = \text{constant} , \quad (2.48)$$

follows then as a consequence of the invariance of the governing equations under the variations (2.38) (infinitesimal rotations).

iii. *Energy evolution.* Since the focus in this work is on the contact contributions, we consider without loss of generality the case defined by two hyperelastic solids characterized by the stored energy functions  $W^{(i)}(\mathbf{C}^{(i)})$  in terms of the right Cauchy-Green tensor  $\mathbf{C}^{(i)} = \mathbf{F}^{(i)T} \mathbf{F}^{(i)}$  ( $i = 1, 2$ ) by frame indifference. The second Piola-Kirchhoff stress tensor is then given by the usual relation

$$\mathbf{S}^{(i)} = 2 \frac{\partial W^{(i)}}{\partial \mathbf{C}^{(i)}} , \quad (2.49)$$

for  $i = 1, 2$ . In this case, the total energy of the system of solids is given by

$$\mathcal{E}_t := \sum_{i=1}^2 \left\{ \underbrace{\int_{\Omega^{(i)}} \rho_o^{(i)} \|\mathbf{V}^{(i)}\|^2 d\Omega^{(i)}}_{\text{kinetic energy}} + \underbrace{\int_{\Omega^{(i)}} W^{(i)} d\Omega^{(i)}}_{\text{strain energy}} \right\} , \quad (2.50)$$

for a given time  $t$ .

The evolution of the total energy of the system of solids is easily obtained by inserting  $\mathbf{V}^{(i)}$  in the test function slot  $\delta \boldsymbol{\varphi}^{(i)}$  of (2.20). Carrying on this operation, the rate of change of the total energy is given by

$$\dot{\mathcal{E}}_t = \underbrace{\int_{\Gamma^{(1)}} p \dot{g} d\Gamma^{(1)}}_{:= \dot{\mathcal{E}}_{c_N}} - \underbrace{\int_{\Gamma^{(1)}} t_{T\alpha} \dot{\xi}^\alpha d\Gamma^{(1)}}_{:= \dot{\mathcal{E}}_{c_T}} , \quad (2.51)$$

where we have extended the integrals over  $\Gamma^{(1)}$  since the integrands vanish outside  $\Gamma_{c,t}^{(1)}$ . The case of a free system of solids as defined by (2.36) is considered again. The normal contact component vanishes by (2.30), that is,

$$\dot{\mathcal{E}}_{c_N} = 0 , \quad (2.52)$$

showing the conservative character of the normal contact interaction. On the other hand, denoting by  $\|\mathbf{t}_t\|_{ref}^2 := t_{T\alpha} M^{\alpha\beta} t_{T\beta}$  (i.e., the norm in the convected reference frame), the tangential contact component leads to

$$\dot{\mathcal{E}}_{c_T} = - \underbrace{\int_{\Gamma^{(1)}} \mu p \gamma \left( \frac{\|\mathbf{t}_T\|_{ref}}{\|\mathbf{t}_T\|} \right)^2 d\Gamma^{(1)}}_{:= \mathcal{D}_{frict} \geq 0} \leq 0 , \quad (2.53)$$

given (2.29)<sub>1</sub> and (2.34)<sub>1</sub>. The inequality (2.53) shows the dissipative character of the frictional problem. Therefore, we conclude that

$$\boxed{\dot{\mathcal{E}}_t = -\mathcal{D}_{frict} \leq 0 \quad \implies \quad \mathcal{E}_t \leq \mathcal{E}_o \quad \forall t,} \quad (2.54)$$

for an initial energy  $\mathcal{E}_o$ . The energy inequality (2.54) defines an *a-priori stability estimate* to be preserved by the numerical scheme. The goal is then the formulation of time-stepping algorithms exhibiting positive energy dissipation (or, simply, *dissipative schemes*), and momentum-conserving as shown by (2.40) and (2.48) for the continuum system.

**Remark 2.1.** A fully spatial formulation of Coulomb friction is obtained by replacing the reference metric  $M_{\alpha\beta}$  in the definition (2.32) of the slip velocity  $\mathbf{v}$  with the spatial metric  $m_{\alpha\beta}$ . In this case, a straightforward calculation shows that the frictional dissipation (2.53) reads

$$\mathcal{D}_{frict} = \int_{\Gamma^{(1)}} \mu p \gamma \, d\Gamma^{(1)} \geq 0. \quad (2.55)$$

Similarly, the convected form of Coulomb law (see LAURSEN [1994]) is obtained by evaluating the norms of the tangential traction in (2.31) and (2.33) with the reference metric (i.e.,  $\|\mathbf{t}_t\|_{ref}$  as defined above), while maintaining the definition (2.32). In this case also, the frictional dissipation is given by (2.55).  $\square$

### 3. A Dissipative Time-Stepping Algorithm for Frictional Contact

We describe in this section the formulation of a new time-stepping algorithm for general frictional contact problems that exhibits the a-priori stability estimate (2.54) derived in the previous section for the continuum problem. As a consequence, the final scheme is unconditionally dissipative in the sense that the energy of the system of solids never exceeds its initial value. The approximation of the normal part has been presented recently in ARMERO & PETŐCZ [1996] by the authors and it is summarized in Section 3.2. A treatment of the frictional contributions leading to positive dissipation is introduced in Section 3.3.

#### 3.1. Temporal discretization. Momentum conservation and energy evolution

We consider a temporal discretization of the equations described in the previous section for the interval  $[0, T] = \cup_n \{t_n, t_{n+1}\}$ . Let  $\{t_n, t_{n+1}\}$  denote a typical time increment, with time step  $\Delta t = t_{n+1} - t_n$ . Denote by  $\varphi_n \approx \varphi_{t_n}$  and by  $\mathbf{V}_n \approx \mathbf{V}_{t_n}$ , that is, time discrete approximations of the deformation and velocity fields, respectively. With this notation, we

consider the following mid-point temporal discretization of the governing equations (2.20)

$$\left. \begin{aligned} \frac{\varphi_{n+1}^{(i)} - \varphi_n^{(i)}}{\Delta t} &= \mathbf{V}_{n+\frac{1}{2}}^{(i)} \quad i = 1, 2, \\ \sum_{i=1}^2 \left\{ \int_{\Omega^{(i)}} \left[ \rho_o^{(i)} \frac{\mathbf{V}_{n+1}^{(i)} - \mathbf{V}_n^{(i)}}{\Delta t} \cdot \delta \boldsymbol{\varphi}^{(i)} + \widehat{\mathbf{S}}^{(i)} : \mathbf{F}_{n+\frac{1}{2}}^{(i)T} \text{Grad}(\delta \boldsymbol{\varphi}^{(i)}) \right] d\Omega^{(i)} \right. \\ &\quad \left. - \int_{\Omega^{(i)}} \rho_o^{(i)} \mathbf{b}_{n+\frac{1}{2}}^{(i)} \cdot \delta \boldsymbol{\varphi}^{(i)} d\Omega^{(i)} - \int_{\Gamma_T^{(i)}} \hat{\mathbf{t}}_{n+\frac{1}{2}}^{(i)} \cdot \delta \boldsymbol{\varphi}^{(i)} d\Gamma^{(i)} \right\} \\ &\quad + \int_{\Gamma_c^{(1)}} [-\hat{p} \delta g + \hat{t}_{T\alpha} \delta \xi^\alpha] d\Gamma^{(1)} = 0, \end{aligned} \right\} \quad (3.1)$$

in the mid-point configuration

$$\boldsymbol{\varphi}_{n+\frac{1}{2}} := \frac{1}{2} (\boldsymbol{\varphi}_n + \boldsymbol{\varphi}_{n+1}), \quad (3.2)$$

and the mid-point velocities

$$\mathbf{V}_{n+\frac{1}{2}} = \frac{1}{2} (\mathbf{V}_n + \mathbf{V}_{n+1}). \quad (3.3)$$

The time discrete variations of the gap and the slip in (3.1) are defined accordingly by

$$\delta g := \left[ \delta \boldsymbol{\varphi}^{(1)}(\mathbf{X}) - \delta \boldsymbol{\varphi}^{(2)}(\mathbf{Y}_{n+\frac{1}{2}}(\mathbf{X})) \right] \cdot \boldsymbol{\nu}_{n+\frac{1}{2}}, \quad (3.4)$$

and

$$\begin{aligned} A_{\alpha\beta} g_{n+\frac{1}{2}} \delta \xi^\beta &= \left[ \delta \boldsymbol{\varphi}^{(1)}(\mathbf{X}) - \delta \boldsymbol{\varphi}^{(2)}(\mathbf{Y}_{n+\frac{1}{2}}(\mathbf{X})) \right] \cdot \boldsymbol{\tau}_{\alpha n+\frac{1}{2}} \\ &\quad + g_{n+\frac{1}{2}} \delta \boldsymbol{\varphi}_{,\alpha}^{(2)}(\mathbf{Y}_{n+\frac{1}{2}}(\mathbf{X})) \cdot \boldsymbol{\nu}_{n+\frac{1}{2}}, \end{aligned} \quad (3.5)$$

for a material point  $\mathbf{X} \in \Gamma^{(1)}$ , in terms of the closest-point projection  $\mathbf{Y}_{n+\frac{1}{2}} = \hat{\mathbf{Y}}_{n+\frac{1}{2}}(\mathbf{X})$  evaluated at the mid-point configuration (3.2). This closest-point projection defines also the geometric quantities  $\boldsymbol{\nu}_{n+\frac{1}{2}}$ ,  $\boldsymbol{\tau}_{\alpha n+\frac{1}{2}}$ , and the gap  $g_{n+\frac{1}{2}}$  as given by (2.3). The discrete approximations  $\widehat{\mathbf{S}}^{(i)}$ ,  $\hat{p}$ , and  $\hat{t}_{T\alpha}$  for the stresses, normal pressure and tangential frictional tractions, respectively, are to be defined. The interest herein is the development of approximations such that the conservation and dissipation properties identified in Section 2.3 are inherited by the numerical scheme. We have written again the contact contributions in (3.1) with the whole boundary  $\Gamma^{(1)}$  as domain of integration, since the integrands ( $\hat{p}$  and

$\hat{t}_{T\alpha}$ ) are imposed to vanish outside the contact boundary. We refer to the Appendix for complete details on the finite element implementation of the above considerations.

i. *Conservation of linear momentum.* The conservation of linear momentum for the case of a free system of solids (i.e., satisfying (2.36) at the mid-point configuration (3.2) as needed in (3.1)) follows as for the continuum system by considering the translations (2.38) in the variations of (3.1). We conclude that

$$\mathbf{L}_n = \mathbf{L}_{n+1} , \quad (3.6)$$

for a typical time step  $\{t_n, t_{n+1}\}$ .

ii. *Conservation of angular momentum.* Following the arguments presented in Section 2.3 for the continuum problem, consider variations consisting of the infinitesimal rotations

$$\delta\varphi^{(i)} = \mathbf{w} \times \varphi_{n+\frac{1}{2}}^{(i)} \quad i = 1, 2 , \quad (3.7)$$

for  $\mathbf{w} \in \mathbb{R}^{n_{\text{dim}}}$ . We first note that the gap and slip variations, given respectively by (3.4) and (3.5), vanish for the variations (3.7). The arguments presented in (2.45) and (2.46) for the continuum system apply here for the time discrete case. We note that the consideration of the geometric quantities of the contact terms in the mid-point configuration, and in particular the closest-point projection, shows to be crucial for these arguments to apply. The introduction of (3.7) into (3.1)<sub>2</sub>, in combination of the vector identity

$$\begin{aligned} \varphi_{n+\frac{1}{2}}^{(i)} \times (\mathbf{V}_{n+1}^{(i)} - \mathbf{V}_n^{(i)}) &= \varphi_{n+1}^{(i)} \times \mathbf{V}_{n+1}^{(i)} - \varphi_n^{(i)} \times \mathbf{V}_n^{(i)} \\ &\quad - (\varphi_{n+1}^{(i)} - \varphi_n^{(i)}) \times \mathbf{V}_{n+\frac{1}{2}}^{(i)} \quad i = 1, 2 , \end{aligned} \quad (3.8)$$

the last term vanishing by (3.1)<sub>1</sub>, and the relation (2.43) with  $\mathbf{F}_{n+\frac{1}{2}}^{(i)}$  by (3.7), leads to

$$(\mathbf{J}_{n+1} - \mathbf{J}_n) \cdot \mathbf{w} = - \sum_{i=1}^2 \int_{\Omega^{(i)}} \widehat{\mathbf{S}}^{(i)} : \widehat{\mathbf{W}} \, d\Omega^{(i)} = 0 , \quad (3.9)$$

if we impose the symmetry condition for the stresses  $\widehat{\mathbf{S}}^{(i)}$  ( $i = 1, 2$ ), as for the continuum case. The conservation of angular momentum for a free system of solids

$$\mathbf{J}_n = \mathbf{J}_{n+1} , \quad (3.10)$$

for the discrete equations (3.1) follows. For our purposes, the momentum-conserving character of the discrete contact contributions, regardless of the actual approximations  $\hat{p}$  and  $\hat{t}_T$ , is to be noted.



iii. *Energy evolution.* The evolution of the energy for the discrete equations (3.1) follows by considering the variations

$$\delta\varphi^{(i)} = \varphi_{n+1}^{(i)} - \varphi_n^{(i)} \quad i = 1, 2. \quad (3.11)$$

The energy-conserving approximation  $\widehat{\mathbf{S}}^{(i)}$  of the stresses presented in SIMO & TARNOV [1992] is considered, leading to the expression

$$\widehat{\mathbf{S}}^{(i)} = \frac{1}{2}\mathbf{C}^{(i)}(\mathbf{E}_{n+1}^{(i)} + \mathbf{E}_n^{(i)}) \quad i = 1, 2, \quad (3.12)$$

for a Saint-Venant Kirchhoff model characterized by the constant material tangent  $\mathbf{C}$  and the Green-Lagrange strain tensor  $\mathbf{E} = (\mathbf{C} - \mathbf{1})/2$ . The symmetry of  $\widehat{\mathbf{S}}^{(i)}$  is to be noted. Expressions for general elastic models can be found in GONZALEZ & SIMO [1995]. The introduction of (3.11) in (3.1) leads to the evolution of energy equation for the discrete problem

$$\Delta\mathcal{E}\Big|_n^{n+1} = \Delta\mathcal{E}_{c_N}\Big|_n^{n+1} + \Delta\mathcal{E}_{c_T}\Big|_n^{n+1}, \quad (3.13)$$

identifying the change of energy in a typical time step  $\{t_n, t_{n+1}\}$  in a free system of solids as arising from the contact terms, the normal and tangential parts, respectively. We consider each contribution separately in the next sections.

### 3.2. A conserving approximation of the normal contact pressure

The introduction of the variations (3.11) in the normal contact term in (3.1) leads to the expression

$$\Delta\mathcal{E}_{c_N}\Big|_n^{n+1} = \int_{\Gamma^{(1)}} \hat{p} (g_{n+1}^d - g_n^d) d\Gamma^{(1)}, \quad (3.14)$$

where, after using (3.4),

$$\boxed{g_{n+1}^d(\mathbf{X}) = g_n^d(\mathbf{X}) + \nu_{n+\frac{1}{2}} \cdot \left[ \left( \varphi_{n+1}^{(1)}(\mathbf{X}) - \varphi_n^{(1)}(\mathbf{X}) \right) - \left( \varphi_{n+1}^{(2)}(\hat{\mathbf{Y}}_{n+\frac{1}{2}}(\mathbf{X})) - \varphi_n^{(2)}(\hat{\mathbf{Y}}_{n+\frac{1}{2}}(\mathbf{X})) \right) \right]}, \quad (3.15)$$

for a material point  $\mathbf{X} \in \Gamma^{(1)}$ . The evolution equation (3.15) is initialized with the last (real) gap  $g_n$  previous to the first time-step in contact, detected by an initial negative (real) gap  $g_{n+1}$ . We refer to  $g^d$  as the *dynamic gap*. The difference of  $g_{n+1}^d$  and the gap  $g_{n+1}$  defined by the closest-point projection (2.2) at the configuration  $\varphi_{n+1}$ , as employed in standard numerical treatments of the problem, is to be noted. In this respect, we observe that (3.15) defines a second-order approximation of the evolution equation (2.17). The evaluation of the deformations  $\varphi_{n+1}$  and  $\varphi_n$  with the closest-point projection  $\hat{\mathbf{Y}}_{n+\frac{1}{2}}$  at the

mid-point configuration (3.2), defining also the unit normal  $\boldsymbol{\nu}_{n+\frac{1}{2}}$ , is again considered in (3.15) as a consequence of its use in (3.4).

In view of (3.14), we define the contact pressure  $\hat{p}$  by the difference quotient

$$\hat{p} = \begin{cases} -\frac{U(g_{n+1}^d) - U(g_n^d)}{g_{n+1}^d - g_n^d} & \text{if } g_{n+1}^d \neq g_n^d, \\ -U'(\frac{1}{2}(g_{n+1}^d + g_n^d)) & \text{if } g_{n+1}^d = g_n^d, \end{cases} \quad (3.16)$$

for a non-negative penalty regularization potential  $U(g)$ . The numerical simulations in Section 4 consider

$$U(g^d) = \begin{cases} \frac{1}{2} \kappa_N (g^d)^2 & \text{if } g^d \leq 0, \\ 0 & \text{if } g^d \geq 0, \end{cases} \quad (3.17)$$

for a large penalty parameter  $\kappa_N > 0$ . Note that the definition (3.16) is such that  $\hat{p} \geq 0$ . We point out that the contact-release check in (3.16) is performed with the dynamic gap  $g_{n+1}^d$ . Furthermore, since the term  $U(g_n^d)$  vanishes in the first increment in contact, the normal gap constraint (2.4) is imposed effectively at  $t_{n+1}$  (not at the mid-point) as  $\kappa_N \rightarrow \infty$ , leading to an improved numerical performance of the scheme. Similarly, we note that  $\hat{p} > 0$  for the time step of release detected by  $g_{n+1}^d > 0$ .

The change of energy (3.14) in a typical time increment reads then

$$\Delta \mathcal{E}_{c_N} \Big|_n^{n+1} = - \int_{\Gamma^{(1)}} (U_{n+1} - U_n) d\Gamma^{(1)}, \quad (3.18)$$

which implies

$$\Delta (\mathcal{E}_{c_N} + \mathcal{P}) \Big|_n^{n+1} = 0 \quad \text{for} \quad \mathcal{P}_t = \int_{\Omega^{(i)}} U(g_t^d) d\Omega^{(i)} \geq 0. \quad (3.19)$$

For the frictionless case,  $\Delta \mathcal{E}_{c_T} \equiv 0$  in (3.13), so we conclude  $\mathcal{E}_n \leq \mathcal{E}_o$ , for a contact state at  $t_n$ , and  $\mathcal{E}_n = \mathcal{E}_o$ , for a released state at  $t_n$  (since  $\mathcal{P}_n = 0$ ). The restoration of the energy of the system of solids upon release follows in this frictionless case, while the energy is under control during the enforcement of the normal contact constraint, in compliance with the a-priori stability estimate (2.54). Physically, energy is stored in the regularization potential while enforcing the normal contact constraint (2.4), and it is completely restored upon release.

The schemes summarized in this section have been presented recently by the authors for the numerical simulation of frictionless contact in ARMERO & PETŐCZ [1996]. In addition, extensions imposing the derived constraint on the velocity ( $\dot{g} = [\mathbf{V}] \cdot \boldsymbol{\nu} = 0$ ) during persistent contact and modifications exhibiting high-frequency dissipation have been also presented. The reader is referred to this reference for further details. We introduce next

an approximation of the frictional tangential components that inherits the dissipativity of the frictional problem.

### 3.3. A dissipative approximation of the frictional tangential traction

Following a similar strategy as in the previous section, the introduction of the variations (3.11) in the tangential contact term of (3.1) leads to the expression

$$\Delta \mathcal{E}_{cT} \Big|_n^{n+1} = - \int_{\Gamma^{(1)}} \hat{t}_{T\alpha} (\xi_{n+1}^{d,\alpha} - \xi_n^{d,\alpha}) d\Gamma^{(1)}, \quad (3.20)$$

where, after using (3.5),

$$\begin{aligned} A_{\alpha\beta} \nu_{n+\frac{1}{2}} \left( \xi_{n+1}^{d,\beta} - \xi_n^{d,\beta} \right) = & \tau_{\alpha} \nu_{n+\frac{1}{2}} \cdot \left[ \left( \varphi_{n+1}^{(1)}(\mathbf{X}) - \varphi_n^{(1)}(\mathbf{X}) \right) \right. \\ & \left. - \left( \varphi_{n+1}^{(2)}(\hat{\mathbf{Y}}_{n+\frac{1}{2}}(\mathbf{X})) - \varphi_n^{(2)}(\hat{\mathbf{Y}}_{n+\frac{1}{2}}(\mathbf{X})) \right) \right] \\ & + g_{n+\frac{1}{2}} \nu_{n+\frac{1}{2}} \cdot \left( \varphi_{n+1,\alpha}^{(2)}(\hat{\mathbf{Y}}_{n+\frac{1}{2}}(\mathbf{X})) \right. \\ & \left. - \varphi_{n,\alpha}^{(2)}(\hat{\mathbf{Y}}_{n+\frac{1}{2}}(\mathbf{X})) \right). \end{aligned} \quad (3.21)$$

As a consequence of the expression (3.5), the unit normal  $\nu_{n+\frac{1}{2}}$ , the tangent basis  $\tau_{\alpha} \nu_{n+\frac{1}{2}}$ , the (real) gap  $g_{n+\frac{1}{2}}$  and the matrix  $A_{\alpha\beta} \nu_{n+\frac{1}{2}}$  (obtained by (2.19)) are evaluated using the closest-point projection  $\hat{\mathbf{Y}}_{n+\frac{1}{2}}(\mathbf{X})$  given by (2.1) at the mid-point configuration (3.2). The evaluation of the deformations  $\varphi_n^{(i)}$  and  $\varphi_{n+1}^{(i)}$  at this mid-point closest-point, as in the expression (3.15) of the dynamic gap, is to be noted again. The recursive definition (3.21) is initialized by  $\xi_o^\beta \equiv \xi_o^{d,\beta}$  that is, with the position of the closest-point projection in the first iteration detecting contact. We refer to the quantity  $\xi^d$  as the *dynamic slip*. We observe that the time discrete equation (3.21) corresponds to a second order approximation of the continuum rate equation (2.18).

Coulomb friction, as described by equations (2.31) to (2.35), defines a perfect stick/slip response of the interactions between two solids. The constraint of perfect (rigid) stick leads to a difficult enforcement numerically. To integrate these equations, we consider the following new regularization of the slip equation (2.31)

$$\left. \begin{aligned} t_{T\alpha} &= \kappa_T \bar{M}_{\alpha\beta} [\xi^\beta - \bar{\xi}^\beta], \\ M_{\alpha\beta} \dot{\xi}^\beta &= \gamma \frac{t_{T\alpha}}{\|t_T\|}, \end{aligned} \right\} \quad (3.22)$$

for a large penalty parameter  $\kappa_T > 0$ . In the limit  $\kappa_T \rightarrow \infty$ , (3.22)<sub>1</sub> enforces  $\boldsymbol{\xi} = \bar{\boldsymbol{\xi}}$ , which follows the slip relation (3.22)<sub>2</sub>, that is, (2.31). We refer to the point  $\bar{\boldsymbol{\xi}}$  as the *stick point*, and its value is initialized with the initial contact point. In the time discrete setting, we have

$$\bar{\boldsymbol{\xi}} := \boldsymbol{\xi}_o, \quad (3.23)$$

with  $\boldsymbol{\xi}_o \equiv \boldsymbol{\xi}^d$  at  $t_o$  (referring again to the first iteration where contact is detected). The regularized equations (3.22) have a structure similar to the equations of elastoplasticity. We note the use of convected components in (3.22), leading to an invariant regularization. In (3.22)<sub>1</sub>, we have considered  $\bar{M}_{\alpha\beta}$ , the metric at  $\bar{\boldsymbol{\xi}}$ , for simplicity in the numerical equations that follow; see comments below. The regularized equations (3.22) are then integrated numerically using an operator split strategy as developed next.

We discretize the slip relation (3.22) in time through a generalized mid-point approximation of the form

$$\left. \begin{aligned} t_{T\alpha} &= \kappa_T \bar{M}_{\alpha\beta n} \left[ \xi_{n+1}^{d,\beta} - \bar{\xi}_n^{d,\beta} \right], \\ \bar{M}_{\alpha\beta n} \left( \bar{\xi}_{n+1}^{d,\beta} - \bar{\xi}_n^{d,\beta} \right) &= \Delta\gamma \frac{t_{T\alpha_{n+\vartheta}}}{\|t_{T_{n+\vartheta}}\|}, \end{aligned} \right\} \quad (3.24)$$

with

$$t_{T\alpha_{n+\vartheta}} := \vartheta t_{T\alpha_{n+1}} + (1 - \vartheta) t_{T\alpha_n}, \quad (3.25)$$

for a numerical parameter  $\vartheta \in (0, 1]$ . Note the use of the dynamic slips in (3.25). We have considered an explicit approximation at  $\bar{\boldsymbol{\xi}}_n^d$  of the reference metric  $\bar{M}_{\alpha\beta}$ . The need of this approximation in the proof of the dissipativity of the scheme, as developed below, arises from the hypo-elastic character of the regularization (3.22)<sub>1</sub>, unless  $\bar{M}_{\alpha\beta}$  is constant. In fact, for a constant metric  $M_{\alpha\beta} \equiv \bar{M}_{\alpha\beta}$ , the hyper-elastic relation

$$t_\alpha = \frac{\partial}{\partial \xi^\alpha} \left( \frac{1}{2} \kappa_T \xi^\delta \bar{M}_{\delta\beta} \xi^\beta \right), \quad (3.26)$$

is recovered for the regularized stick phase, identifying a quadratic energy potential for the regularization (3.22). Given the small slips during the stick phase (enforced to vanish in the limit  $\kappa_T \rightarrow \infty$ ), and the simplicity of the resulting discrete equations, we view this approximation as a simplification of the final equations rather than a limitation.

The unknown tangential traction  $t_{T_{n+\vartheta}}$  is constrained by the slip surface (2.33), defining the discrete stick/slip and consistency conditions

$$\phi = \|t_{T_{n+\vartheta}}\| - \mu \hat{p} \leq 0, \quad (3.27)$$

$$\Delta\gamma \geq 0, \quad \text{and} \quad \Delta\gamma \phi = 0. \quad (3.28)$$

The pressure  $\hat{p}$  defined by (3.16) has been used in (3.27). The Euclidean norms in (3.24) and (3.28) are computed following the continuum relation (2.35). The value  $\vartheta = 1/2$  is

preferred, since it leads to a second-order accurate scheme (for constant  $M_{\alpha\beta}$ ), and the availability of the metric  $m_{\alpha\beta}_{n+\frac{1}{2}}$  from the closest-point projection  $\mathbf{Y}_{n+\frac{1}{2}}$ .

The discrete slip equations (3.24), (3.27), and (3.28) are solved for the tangential traction  $\mathbf{t}_{T_{n+\vartheta}}$  using an operator split with an structure similar to return mapping algorithms in elastoplasticity (see SIMO & HUGHES [1997]). In this setting, define the trial state

$$\boxed{\mathbf{t}_{T_{\alpha}}^{trial}{}_{n+\vartheta} := \kappa_T \bar{M}_{\alpha\beta n} \left( \xi_{n+\vartheta}^{d,\beta} - \bar{\xi}_n^{d,\beta} \right)}, \quad (3.29)$$

and compute the trial slip function

$$\phi^{trial} := \|\mathbf{t}_{T_{n+\vartheta}}^{trial}\| - \mu \hat{p}, \quad (3.30)$$

for the contact pressure  $\hat{p} \geq 0$  given by (3.16). The case  $\phi^{trial} \leq 0$  corresponds to a *stick step*, with the update equations

$$\mathbf{t}_{T_{n+\vartheta}} = \mathbf{t}_{T_{n+\vartheta}}^{trial}, \quad \text{and} \quad \bar{\xi}_{n+1}^d = \bar{\xi}_n^d, \quad (3.31)$$

for the tangential traction and stick point, respectively.

A frictional slip step is detected with  $\phi^{trial} > 0$ . In this case, we must have frictional slip  $\Delta\gamma > 0$  which is found by rewriting (3.24)<sub>2</sub> as

$$\mathbf{t}_{T_{\alpha_{n+\vartheta}}}^{trial} = \kappa_T \vartheta \Delta\gamma \frac{\mathbf{t}_{T_{\alpha_{n+\vartheta}}}}{\|\mathbf{t}_{T_{n+\vartheta}}\|} + \mathbf{t}_{T_{\alpha_{n+\vartheta}}}, \quad (3.32)$$

after a simple calculation involving the definition of the trial traction (3.29). The equation (3.32) implies

$$\|\mathbf{t}_{T_{n+\vartheta}}^{trial}\| = \|\mathbf{t}_{T_{n+\vartheta}}\| + \kappa_T \vartheta \Delta\gamma, \quad (3.33)$$

and

$$\frac{\mathbf{t}_{T_{n+\vartheta}}^{trial}}{\|\mathbf{t}_{T_{n+\vartheta}}^{trial}\|} = \frac{\mathbf{t}_{T_{n+\vartheta}}}{\|\mathbf{t}_{T_{n+\vartheta}}\|}. \quad (3.34)$$

The imposition of the consistency condition (3.28)<sub>2</sub>

$$\phi = \|\mathbf{t}_{T_{n+\vartheta}}\| - \mu \hat{p} = 0, \quad (3.35)$$

leads in combination with (3.30) and (3.33) to

$$\Delta\gamma = \frac{\phi^{trial}}{\vartheta \kappa_T} > 0, \quad (3.36)$$

in a frictional slip step. Furthermore, (3.32), (3.34) and (3.35) result in

$$\boxed{\mathbf{t}_{T_{n+\vartheta}} = \mu \hat{p} \frac{\mathbf{t}_{T_{n+\vartheta}}^{trial}}{\|\mathbf{t}_{T_{n+\vartheta}}^{trial}\|}}. \quad (3.37)$$

**TABLE 3.1.** Summary of the discrete equations for the frictional contributions. (The subindices  $n + \vartheta$  for the traction and  $n$  for the stick point have been omitted, since their consideration is not required in the actual numerical implementation)

<p>For a contact step (i.e., <math>\hat{p} &gt; 0</math> as defined by (3.16)), and a given <math>\xi_n^d</math>, define <math>\xi_{n+1}^d</math> by (3.21).</p> <p>For a given stick point <math>\bar{\xi}^d</math>, define the trial tangential traction</p> $\hat{t}_{T\alpha}^{trial} := \kappa_T \bar{M}_{\alpha\beta} \left( \xi_{n+\vartheta}^{d,\beta} - \bar{\xi}^{d,\beta} \right),$ <p>for <math>\xi_{n+\vartheta}^d := \vartheta \xi_{n+1}^d + (1 - \vartheta) \xi_n^d</math>, with the metric <math>\bar{M}_{\alpha\beta}</math> evaluated at the stick point <math>\bar{\xi}^d</math>. Compute the trial slip surface</p> $\phi^{trial} := \ \hat{t}_T^{trial}\  - \mu\hat{p}.$ <p>IF ( <math>\phi^{trial} \leq 0</math> ) THEN</p> $\hat{t}_T = \hat{t}_T^{trial}, \quad (\text{stick step})$ <p>ELSE</p> $\hat{t}_T = \mu\hat{p} \frac{\hat{t}_T^{trial}}{\ \hat{t}_T^{trial}\ }, \quad (\text{frictional slip step})$ <p>and update the stick point by <math>\bar{\xi}^d \leftarrow \xi_{n+1}^d</math>.</p> <p>ENDIF</p>
---

After a frictional slip step, equation (3.24)<sub>2</sub> defines a new stick point  $\bar{\xi}_{n+1}^d$ . However, we consider the stick point defined by the update  $\bar{\xi}_{n+1}^d = \xi_{n+1}^d$  (that is, the exact limit solution) in the step following the frictional slip, similar to the original initialization (3.23) of the stick point and instead of the value given by (3.24)<sub>2</sub>. This modification is crucial for the final dissipativity of the scheme, as shown in the following section. Furthermore, it avoids possible drifts of the stick point with respect to the path of the contact point  $\xi_{n+1}^d$  that may occur for finite values of  $\kappa_T$ . The predictor/corrector scheme is simply repeated from the new stick point. We view this modification as part of the definition of the penalty regularization proposed herein by (3.22).

The tangential traction  $\hat{t}_T = t_{T_{n+\vartheta}}$  (given by (3.29) or (3.37) for a stick or frictional step, respectively) is entered in the discrete weak form (2.20). The above developments are summarized in Table 3.2. The subindices  $n + \vartheta$  for the traction  $t_T$  and  $n$  for the stick point

have been omitted for clarity, since they are not required in the actual implementation. According to the developments in Section 3.1, the final algorithm conserves linear and angular momentum. We show next that the proposed scheme leads to a positive energy dissipation, thus conforming with the a-priori stability estimate (2.54).

### 3.3.1. The dissipative properties of the proposed scheme

To prove the dissipativity of the frictional algorithm described in the previous section, we consider the general case given by a sequence of  $N \geq 0$  stick steps followed by either release or frictional slip. Let

$$\boldsymbol{\eta}_n^d := \boldsymbol{\xi}_n^d - \bar{\boldsymbol{\xi}}^d, \quad (3.38)$$

for stick point  $\bar{\boldsymbol{\xi}}^d := \boldsymbol{\xi}_o^d$  during the considered  $N + 1$  steps, and

$$\|\boldsymbol{\eta}_n^d\|_M^2 := \bar{M}_{\alpha\beta} \eta_n^{d,\alpha} \eta_n^{d,\beta}. \quad (3.39)$$

for the constant metric  $\bar{M}_{\alpha\beta}$  at  $\bar{\boldsymbol{\xi}}^d$ .

The discrete change of energy (3.20) due to the tangential frictional contributions for a *stick step*  $\{t_n, t_{n+1}\}$  is given by

$$\begin{aligned} \Delta \mathcal{E}_{c_T} \Big|_n^{n+1} &= - \int_{\Gamma^{(1)}} \kappa_T (\xi_{n+\vartheta}^{d,\alpha} - \bar{\xi}_n^{d,\alpha}) \bar{M}_{\alpha\beta_n} (\xi_{n+1}^{d,\beta} - \xi_n^{d,\beta}) d\Gamma^{(1)} \\ &= - \int_{\Gamma^{(1)}} \kappa_T \eta_{n+\vartheta}^{d,\alpha} \bar{M}_{\alpha\beta_n} (\eta_{n+1}^{d,\beta} - \eta_n^{d,\beta}) d\Gamma^{(1)} \\ &= - \int_{\Gamma^{(1)}} \left[ \frac{\kappa_T}{2} \|\boldsymbol{\eta}_{n+1}^d\|_M^2 - \frac{\kappa_T}{2} \|\boldsymbol{\eta}_n^d\|_M^2 + \kappa_T (\vartheta - \frac{1}{2}) \|\boldsymbol{\eta}_n^d - \boldsymbol{\eta}_{n+1}^d\|_M^2 \right] d\Gamma^{(1)}, \end{aligned} \quad (3.40)$$

after using (3.29) and the vector identity

$$\boldsymbol{\eta}_{n+\vartheta}^d = \boldsymbol{\eta}_{n+\frac{1}{2}}^d + (\vartheta - \frac{1}{2}) (\boldsymbol{\eta}_{n+1}^d - \boldsymbol{\eta}_n^d). \quad (3.41)$$

Note again that  $\bar{\boldsymbol{\xi}}_n^d = \bar{\boldsymbol{\xi}}^d$  during the  $N$  stick steps. Therefore, after adding recursively (3.40) for the assumed  $N$  stick step, we have

$$\begin{aligned} \Delta \mathcal{E}_{c_T} \Big|_0^N &= \sum_{n=0}^{N-1} \Delta \mathcal{E}_{c_T} \Big|_n^{n+1} = - \int_{\Gamma^{(1)}} \frac{\kappa_T}{2} \|\boldsymbol{\eta}_N^d\|_M^2 d\Gamma^{(1)} \\ &\quad - (\vartheta - \frac{1}{2}) \sum_{n=0}^{N-1} \int_{\Gamma^{(1)}} \kappa_T \|\boldsymbol{\eta}_n^d - \boldsymbol{\eta}_{n+1}^d\|_M^2 d\Gamma^{(1)} \\ &\leq 0 \quad \text{for } \vartheta \geq 1/2, \end{aligned} \quad (3.42)$$

after noting that  $\|\boldsymbol{\eta}_0^d\|_{\bar{M}} = 0$  since  $\bar{\boldsymbol{\xi}}_o^d = \boldsymbol{\xi}_o^d$ . The estimate (3.42) shows that during the stick phase the total energy of the system of solids does not increase due to the frictional algorithm, i.e., it exhibits *positive dissipation*. If the next step  $\{t_N, t_{N+1}\}$  is a released state (i.e.,  $\hat{p} = 0$  and  $\hat{\mathbf{t}}_T = 0$ ), the above estimate gives the energy dissipated during the contact interval due to the numerical regularization of the tangential traction. This dissipation vanishes as  $\kappa_T \rightarrow \infty$ , i.e., in the limit enforcing the stick constraint  $\|\boldsymbol{\eta}^d\|_{\bar{M}} \rightarrow 0$ .

Similarly, we obtain for the frictional step  $\{t_N, t_{N+1}\}$

$$\begin{aligned} \Delta \mathcal{E}_{c_T} \Big|_N^{N+1} = & - \int_{\Gamma^{(1)}} \frac{\mu \hat{p}}{\|\mathbf{t}_{T_{N+\vartheta}}\|} \left[ \frac{\kappa_T}{2} \|\boldsymbol{\eta}_{N+1}^d\|_{\bar{M}}^2 - \frac{\kappa_T}{2} \|\boldsymbol{\eta}_N^d\|_{\bar{M}}^2 \right. \\ & \left. + \kappa_T \left(\vartheta - \frac{1}{2}\right) \|\boldsymbol{\eta}_N^d - \boldsymbol{\eta}_{N+1}^d\|_{\bar{M}}^2 \right] d\Gamma^{(1)}, \end{aligned} \quad (3.43)$$

after algebraic manipulations as in (3.40), and using (3.37). Adding the equations (3.42) and (3.43), we conclude that for a sequence of  $N$  stick time steps and one frictional step the total change of energy due to the frictional contact contributions is given by

$$\begin{aligned} \Delta \mathcal{E}_{c_T} \Big|_0^{N+1} = & \sum_{n=0}^N \Delta \mathcal{E}_{c_T} \Big|_n^{n+1} \leq - \int_{\Gamma^{(1)}} \frac{\mu \hat{p}}{\|\mathbf{t}_{N+\vartheta}^{trial}\|} \frac{\kappa_T}{2} \|\boldsymbol{\eta}_{N+1}^d\|_{\bar{M}}^2 d\Gamma^{(1)} \\ & - \int_{\Gamma^{(1)}} \left( 1 - \frac{\mu p}{\|\mathbf{t}_{N+\vartheta}^{trial}\|} \right) \frac{\kappa_T}{2} \|\boldsymbol{\eta}_N^d\|_{\bar{M}}^2 d\Gamma^{(1)} \\ & \leq 0 \quad \text{for } \vartheta \geq 1/2, \end{aligned} \quad (3.44)$$

since  $\hat{p} > 0$  and the bracket in the second integral is positive

$$1 - \frac{\mu \hat{p}}{\|\mathbf{t}_{N+\vartheta}^{trial}\|} = \frac{\phi^{trial}}{\|\mathbf{t}_{N+\vartheta}^{trial}\|} > 0. \quad (3.45)$$

by (3.30). The above arguments apply completely to a new series of time steps with the new stick point  $\bar{\boldsymbol{\xi}}^d \leftarrow \boldsymbol{\xi}_{n+1}^d$ . The dissipativity of the proposed frictional algorithm follows.

The derivations of (3.40) and (3.43) involve in a crucial manner the definition (3.21) of the dynamic slip  $\boldsymbol{\xi}^d$ . The combination of the dissipative estimate (3.44) with the conservation property of the normal contact component shows rigorously the unconditional (energy) stability of the proposed contact scheme. The energy in the numerical simulation will never increase over its initial value.

### Remarks 3.1.

1. The fully convected form, as discussed in Remark 2.2, satisfies the above estimates with the norm in  $\|\mathbf{t}_T\|$  replaced by the reference norm  $\|\mathbf{t}_T\|_{ref}$ . Similarly, the fully



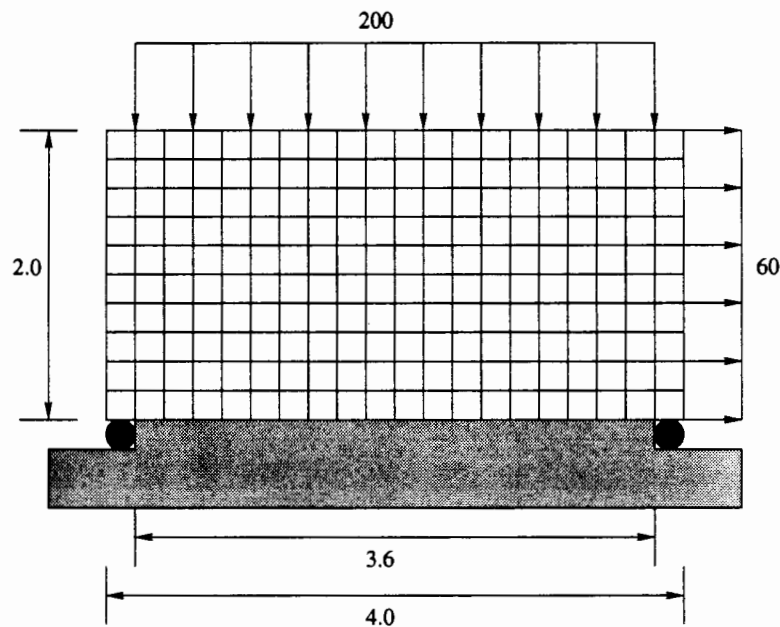


**FIGURE 4.1.** Forging of an elastic block against a rigid foundation. Problem definition.

spatial form of friction leads to the same estimates with spatial norms everywhere. Details are omitted.

2. The proposed scheme applies to both quasi-static and dynamic problems. Note in this respect that the definitions (3.15) and (3.21) of the kinematic quantities  $g^d$  and  $\xi^d$ , respectively, involve the deformations  $\varphi^{(i)}$ , and not the velocities  $V^{(i)}$ . The energy conservation/dissipation properties of the scheme apply in particular to this case (set  $\rho_o^{(i)} \rightarrow 0$  in the above developments), not affecting the contact contributions.  $\square$

## 4. Representative Numerical Simulations.

We present in this section several numerical simulations that assess the performance of the proposed time stepping-algorithms. The examples involve quasi-static and dynamic simulations. Specifically, we present the results obtained for the forging of an elastic block against a rigid foundation in Section 4.1, the impact of two elastic blocks in Section 4.2, the impact of cylinder against a rigid wall in Section 4.3 and, finally, the impact of two elastic cylinders in Section 4.4. We refer to ARMERO & PETŐCZ [1996] for additional examples assessing the performance of the conserving normal contact approximation in frictionless problems.

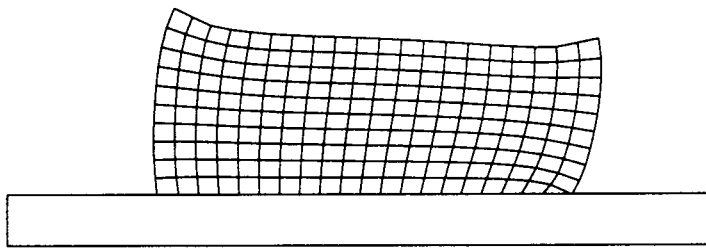


**FIGURE 4.2.** Forging of an elastic block against a rigid foundation. Deformed mesh.

#### 4.1. Forging of an elastic block against a rigid foundation

We consider the benchmark problem presented in ODEN & PIRES [1984] of the forging of an elastic block against a rigid foundation. The purpose of this example is to assess the accuracy of the new frictional integration scheme in a quasi-static setting. As noted in Remark 3.1.2, the numerical integration schemes in time developed in this paper have been presented in terms of the deformations  $\varphi^{(i)}$  of the solids and not the velocities, applying then to the quasi-static case.

The problem definition is depicted in Figure 4.1. An elastic block is pressed against a rigid foundation and pulled by a tangential force uniformly distributed along one of the sides of the block. We have considered the spatial discretization shown in Figure 4.1, with  $20 \times 10$  4-node bilinear quadrilateral finite elements. The material of the block is assumed linear elastic in accordance to the results reported in ODEN & PIRES [1984], with Lamé constants  $\lambda = 576.92$  and  $G = 384.62$ . The linear elastic continuum is recovered in the considerations presented in the previous sections by considering the infinitesimal strain tensor  $\boldsymbol{\varepsilon}(\mathbf{u}) := \text{Grad}^s \mathbf{u}$  in terms of the displacement field  $\mathbf{u}(\mathbf{X}) = \boldsymbol{\varphi}(\mathbf{X}) - \mathbf{X}$ , and the corresponding linear variations, instead of the Green-Lagrange tensor  $\mathbf{E}$  in the elastic term of the governing equations. All the considerations with respect to the evolution of the energy (not the angular momentum due to the lack of invariance of linear elasticity) apply to the infinitesimal continuum, and the corresponding internal force term in the final finite element equations. The finite kinematics of the contact contributions are retained. Plane strain conditions are assumed.

The frictional scheme developed in Section 3 was employed with penalty parameters of  $\kappa_N = 10^8$ ,  $\kappa_T = 10^4$ , and the numerical parameter  $\vartheta = 0.5$  for the frictional contributions. A friction coefficient of  $\mu = 0.5$  is considered. Figure 4.2 shows the deformed configuration for this case. Figure 4.3 depicts the nodal reactions along the base of the block, for both the proposed scheme and the results presented in ODEN & PIRES [1984]. A good agreement between the two curves can be observed, showing an accurate resolution of the frictional interaction of solids in this quasi-static case by the proposed algorithm. We note that,

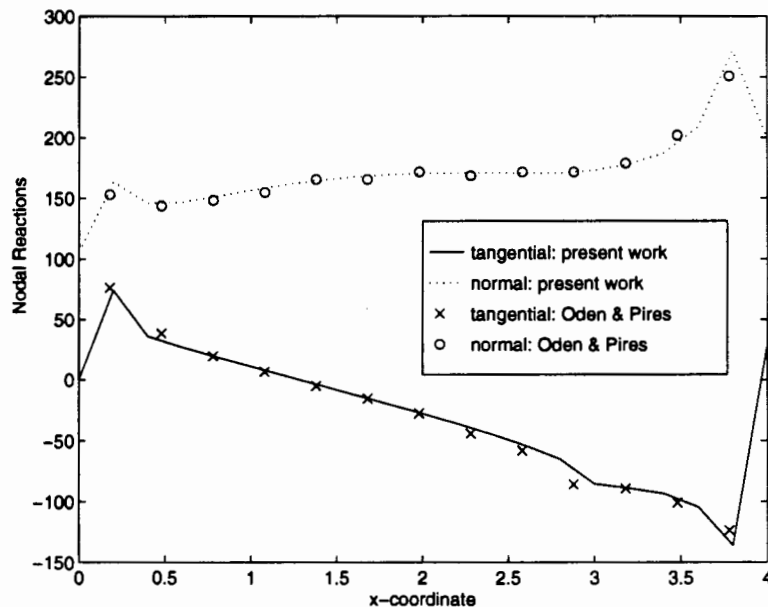


**FIGURE 4.3.** Forging of an elastic block against a rigid foundation. Nodal reactions along the base of the block.

even in this quasi-static case, we consider the mid-point type approximations as developed in Section 3 for the general dynamic problem. Therefore, the solutions obtained with the proposed schemes lead to a positive energy dissipation of the approximation of the frictional forces.

## 4.2. Oblique impact of two infinite blocks

We present in this section the results obtained in the modeling of the oblique impact between two elastic blocks presented in CHEN & YEH [1988]. The problem definition is depicted in Figure 4.4. A rectangular block is given an uniform initial velocity of  $\mathbf{v}_0 = [-10, -10]$  (in a cartesian system as depicted in Figure 4.4), impacting the top surface of a second block whose bottom boundary is fixed. The blocks are modeled with the Saint-Venant Kirchhoff continuum model (3.12). Both blocks are characterized by Lamé constants  $\lambda = 0.0$  and  $G = 500$ , and density  $\rho = 0.1$ . Fully dynamic, plane strain conditions are assumed.

The penalty parameters employed in the simulations are  $\kappa_N = \kappa_T = 10^4$ , with  $\vartheta = 0.5$ . Both frictionless ( $\mu = 0$ ) and frictional ( $\mu = 0.4$ ) cases are considered. A constant time step of  $\Delta t = 0.01$  is employed. Figure 4.5 compares the displacements of point A (see Figure 4.4) obtained in this work with the results reported in CHEN & YEH [1988] for both cases. The horizontal and vertical displacements are plotted versus time. Both displacements and time are measure from the instant of contact between the two blocks. As expected the horizontal displacements are significantly reduced by the presence of friction, while the

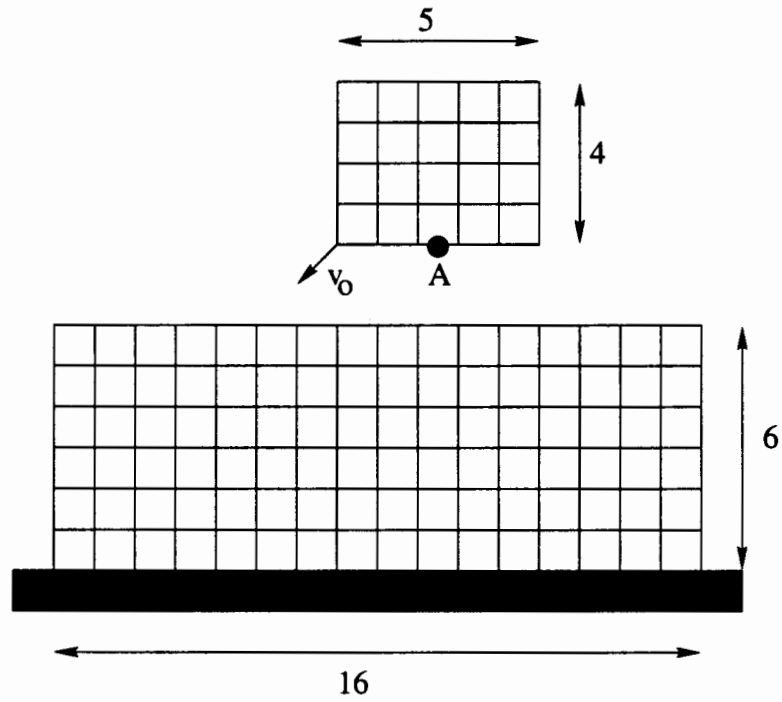


FIGURE 4.4. Oblique impact of two elastic blocks. Problem definition.

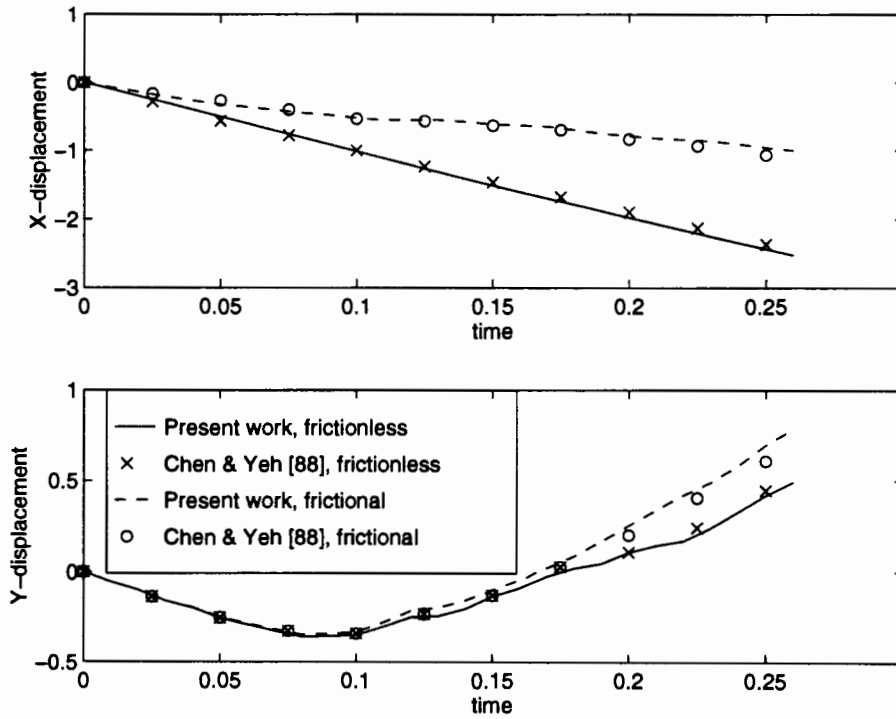
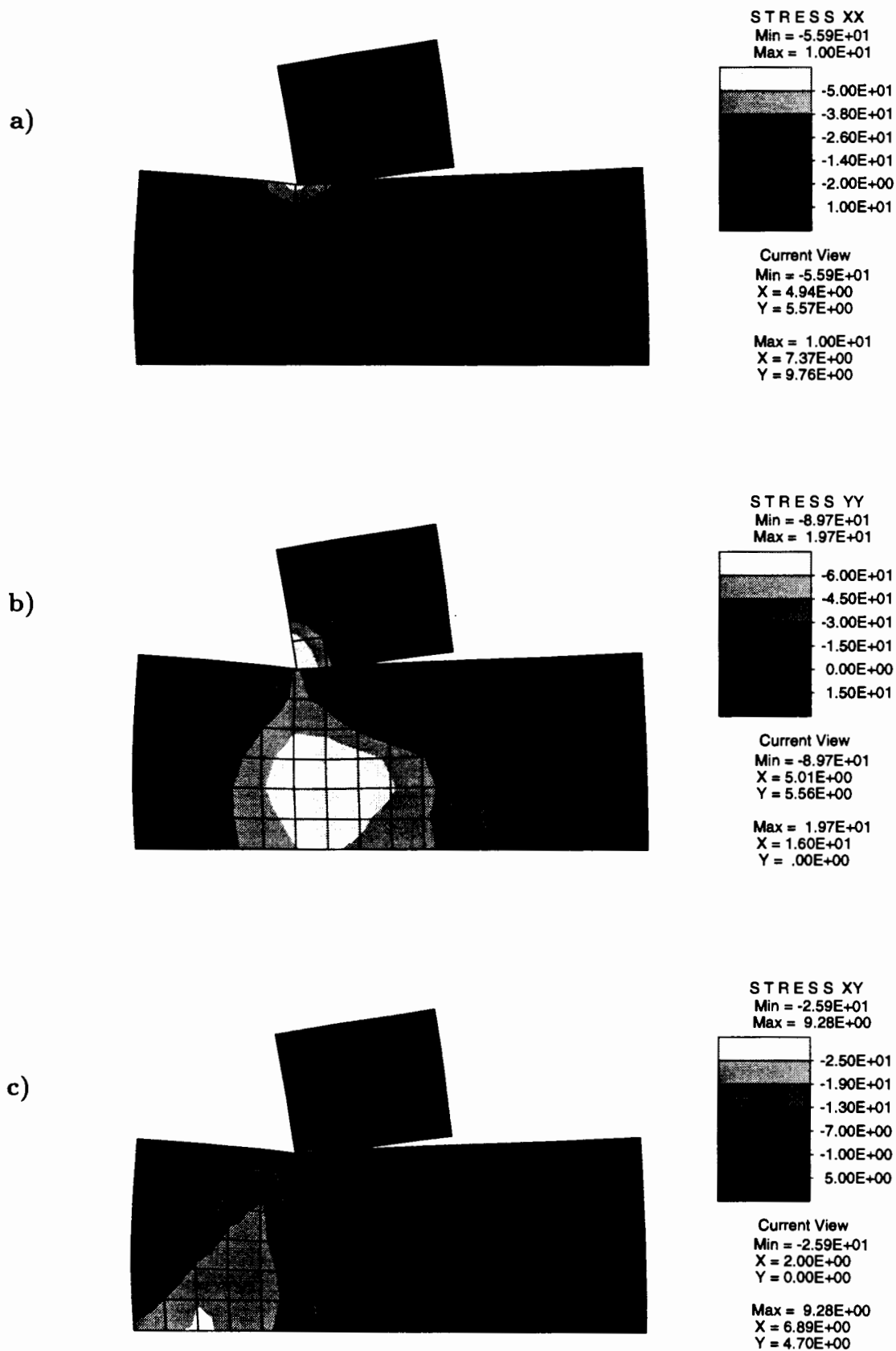


FIGURE 4.5. Oblique impact of two elastic blocks. Displacement of point A (see Figure 4.4) for the frictionless ( $\mu = 0$ ) and frictional ( $\mu = 0.4$ ) cases.



**FIGURE 4.6.** Oblique impact of two elastic blocks. Distribution of the (Cauchy) stresses **a)**  $\sigma_{xx}$ , **b)**  $\sigma_{yy}$ , and **c)**  $\sigma_{xy}$ , at time  $t = 0.12$  (after impact) on the deformed configurations for the frictional case. (The  $x$ -direction is the horizontal direction to the right, with the  $y$ -direction upwards, and origin at the bottom left corner of the block at the bottom)

vertical displacements on the rebound increase when friction is present.

We can observe that the results obtained with the scheme proposed herein compare well with the results presented in CHEN & YEH [1988] for this dynamic contact/impact problem. We have also included in Figure 4.6 the distribution of the stresses  $\sigma_{xx}$ ,  $\sigma_{yy}$  and  $\sigma_{xy}$  (the  $x$  direction being the horizontal direction in Figure 4.4) for the frictional case. All the stresses are shown on top of the deformed configuration of the solids at time  $t = 0.12$ .

### 4.3. Impact of a cylinder on a rigid wall

We present in this section the results obtained in the problem of an elastic cylinder impacting a rigid wall. Fully dynamic simulations are performed, under plane strain conditions. The cylinder of radius  $R = 1.0$  has an uniform initial velocity  $\mathbf{v}_0 = [0.4, -0.4]$  ( $x$  and  $y$  directions corresponding to the horizontal and vertical directions, respectively, in Figures 4.7.a and 4.8.a), impacting the rigid wall at  $45^\circ$ .

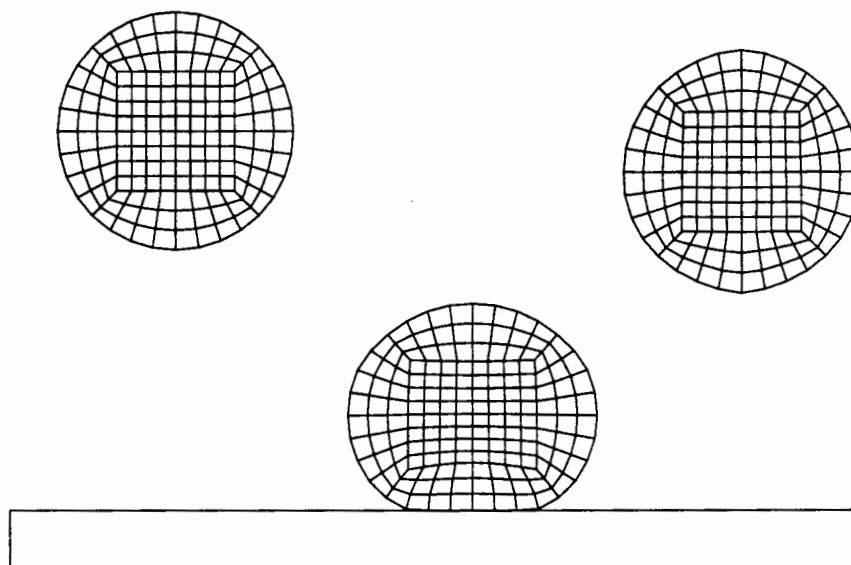
A fully nonlinear elastic model is considered for the cylinder. More specifically, we use the Saint-Venant Kirchhoff model in (3.12) with Lamé constants  $\lambda = 130.0$  and  $G = 43.33$ , and density  $\rho = 8.93$ . Both frictionless and frictional impacts are considered, with a friction coefficient of  $\mu = 0.2$  for the frictional case. The penalty parameters  $\kappa_N = \kappa_T = 10^4$ , and numerical parameter  $\vartheta = 0.5$  for the frictional contributions are employed.

The performance of the time-stepping algorithms presented herein is compared with a traditional mid-point approximation of the contact contributions. In both cases, the energy-conserving scheme (3.12) of SIMO & TARNOW [1992] is considered for the continuum contributions in both cases. The cylinders are discretized with 4-node bilinear finite elements leading to 2-node linear segments to characterize the contact; see Figure 4.7.a. Figures 4.7.a and 4.8.a show the configurations of the cylinder obtained with the proposed scheme before, during, and after contact, for the frictionless and frictional cases, respectively. Finite strains are considered. Notice the additional rotation of the block in the frictional case due to the tangential frictional forces during contact.

Figures 4.7.b and 4.8.b show the total energy evolution during the simulation, for the frictionless and frictional problem respectively. Observe that even in the presence of frictional dissipation, there is an initial increase of the total energy after the impact when using the mid-point rule scheme. This unphysical increase of energy should be contrasted with the dissipation properties shown for the proposed scheme. As expected, the increase of energy for the traditional mid-point scheme is more pronounced in the absence of frictional phenomena, leaving the cylinder with a higher energy content after bouncing. This situation is to be contrasted with the schemes proposed herein. While in contact, the energy of the cylinder is reduced, with the difference in the energy going to the penalty regularization potentials enforcing the impenetrability constraints. As shown in Section 3.2, the total energy of the extended system (the solids and the regularization potentials)

**FRICTIONLESS IMPACT**

a)



b)

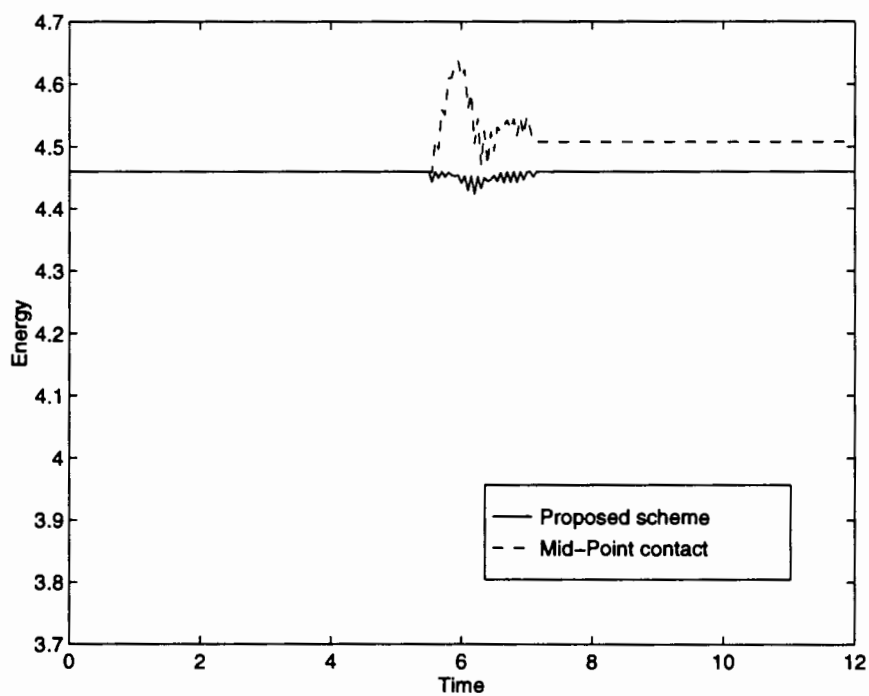
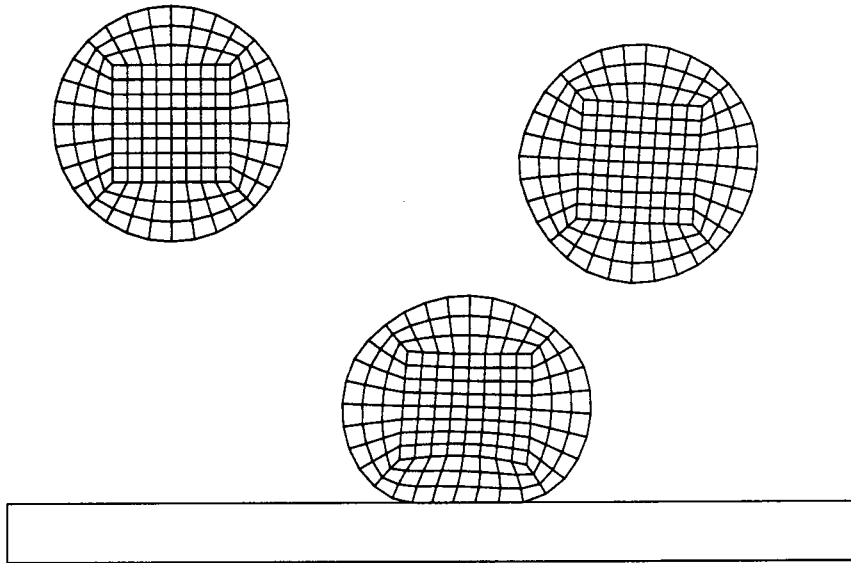


**FIGURE 4.7.** Impact of a circular cylinder on a rigid wall. Solutions obtained with the proposed scheme for frictionless contact. Deformations shown at  $t = 0, 6.3, 12$  (before, during, and after contact, respectively).

**FRICIONAL IMPACT**

a)



b)

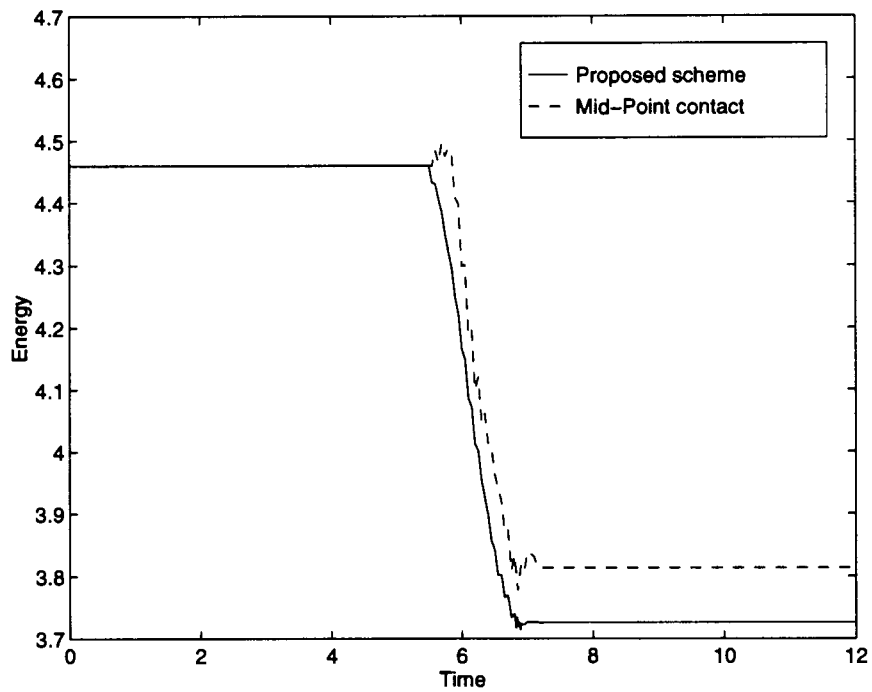


**FIGURE 4.8.** Impact of a circular cylinder on a rigid wall. Solutions obtained with the proposed scheme for frictional contact. Deformations shown at  $t = 0, 6.3, 12$  (before, during, and after contact, respectively).



is always conserved in the frictionless case, leading to the (energy) stability of the scheme. This situation is to be contrasted again with the instability evidenced by standard implicit schemes, like the mid-point rule, in the presence of nonlinearities (unilateral contact constraints, in particular). In addition, we can observe the full restoration of the energy to its initial value upon release in the frictionless case. The lower value in the frictional problems accounts for the physical positive dissipation present in the problem, and modeled by the numerical schemes.

#### 4.4. Skew impact of two elastic cylinders.

This final example considers the free-body system of two nonlinear elastic cylinders impacting at each other. The cylinders have a radius of 1, and are discretized with isoparametric 4-node bilinear finite elements, as shown in Figure 4.9. The center of the left cylinder is located at  $[-1.8, 0.0]$ , while the center of the right cylinder is at  $[1.8, 0.0]$ , in a reference cartesian system. (the  $x$ -direction is the horizontal direction to the right, and the  $y$ -direction is upwards in Figure 4.9). The left cylinder is given an initial velocity  $\mathbf{v}_0 = [1.0, 0.1]$ , while the right cylinder is at rest. We consider 1 time step of  $\Delta t = 1$ , and 250 time steps of  $\Delta t = 0.01$ , for a final time of  $T = 3.5$ . The Saint-Venant Kirchhoff material model (3.12) is assumed for both cylinders with Lamé constants,  $\lambda = 130$ ,  $\mu = 43.33$ , and density  $\rho = 8.93$ . We assume Coulomb friction with  $\mu = 0.2$  with the numerical parameter  $\vartheta = 0.5$ . The penalty parameters for this problem are  $\kappa_N = 10^4$  and  $\kappa_T = 10^3$ .

The continuum contributions to the governing equations are solved using the energy-conserving scheme developed in SIMO & TARNOW [1992], and described in Section 3.1. The contact contributions are approximated with the proposed scheme and the mid-point rule, after noting the mid-point character of the continuum interpolations. Figures 4.9 show the deformed configurations at different times for the proposed scheme. The finite strains that appear in the problem are clear. The evolution of the energy of the cylinders (kinetic plus strain energy) and the different components of the momenta are plotted versus time in Figure 4.10.

The improved stability properties of the newly proposed methods are apparent. The proposed scheme does not show an increase of the energy over the initial value, with the final energy after release being smaller than the origin value due to the frictional dissipation. In contrast, the artificial and unphysical increase in energy for a standard frictional contact scheme, like the midpoint rule, can be observed. In fact, the simulation involving a mid-point contact cannot be continued after  $t = 2.30$ . No convergence is obtained for the given time step. The high value of the energy at this stage is to be noted. Both schemes conserve the momenta (the mid-point contact up to the blow-up of the computation) as the underlying physical system; see Figure 4.10.

The final energy dissipation for the proposed scheme is apparent in Figure 4.10. We

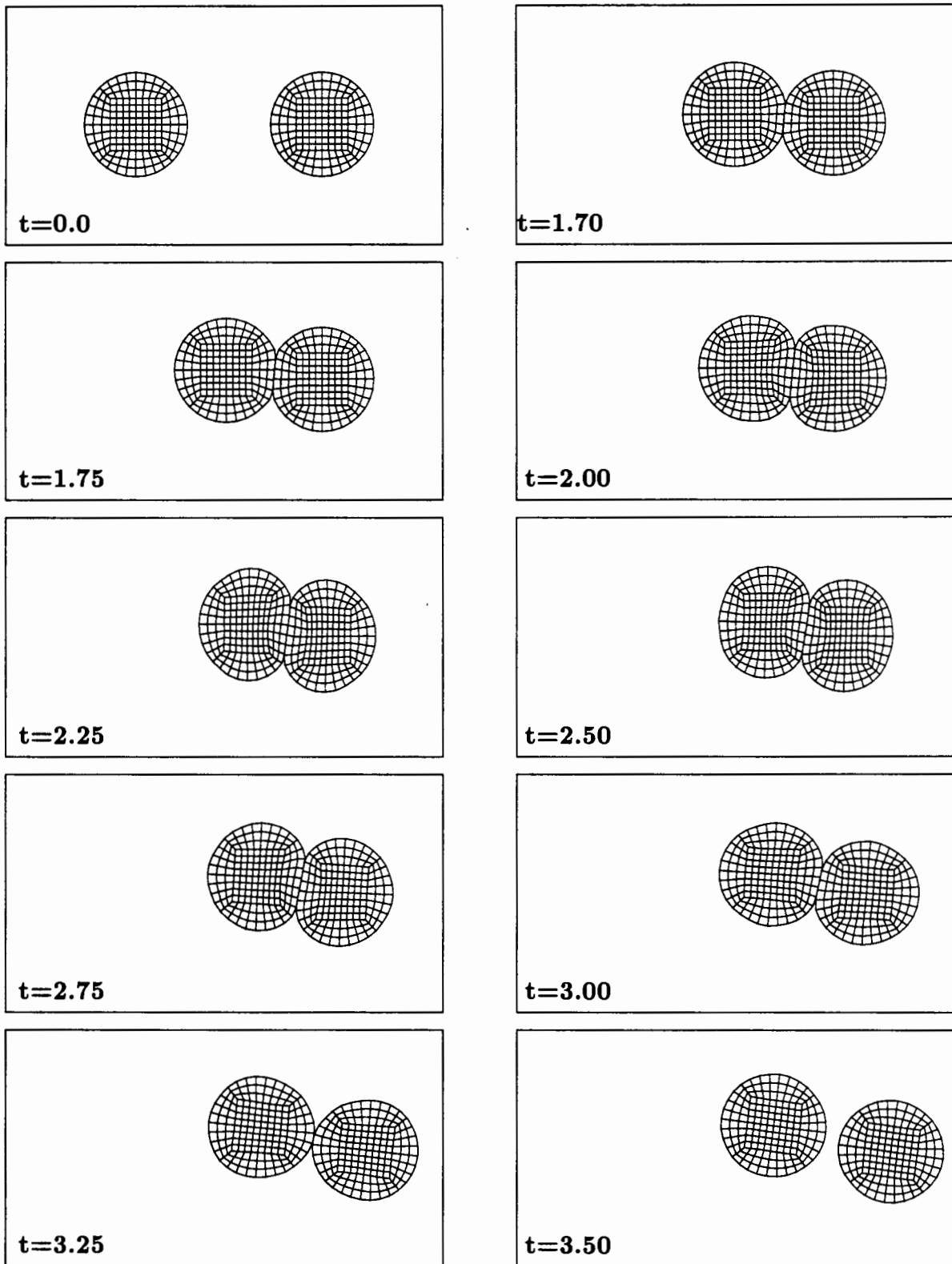


**FIGURE 4.9.** Skew impact of two elastic cylinders. Solutions obtained with the proposed scheme at different times ( $\mu = 0.2$ ).

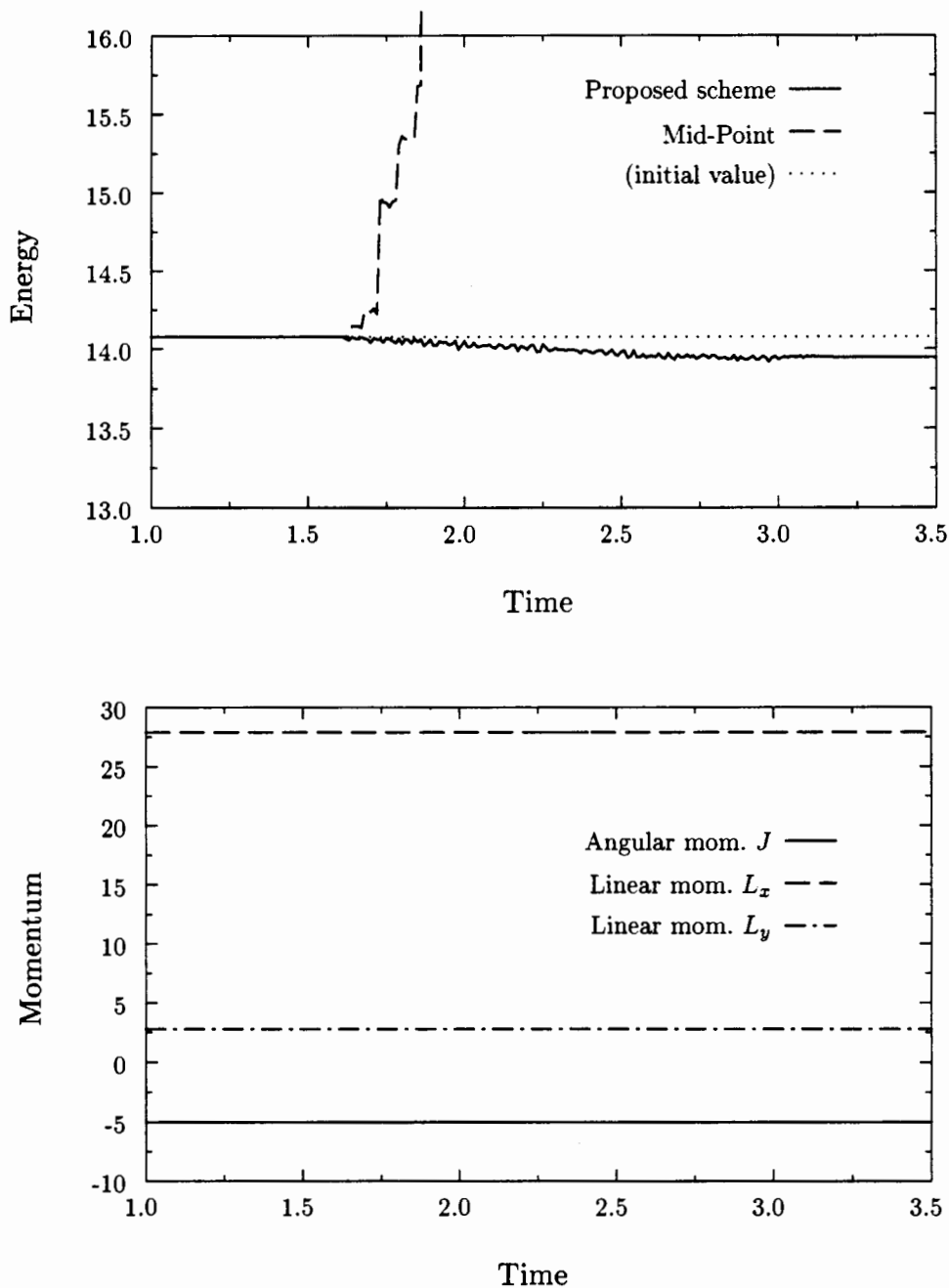


**FIGURE 4.10.** Skew impact of two elastic cylinders. Evolution of the energy, and linear and angular momenta versus time. We can observe the unphysical growth of the energy for the mid-point rule. The computation in this case cannot be continued after  $t = 2.30$  for the given time step  $\Delta t = 0.01$  (no convergence obtained). This situation is to be contrasted with the proposed scheme. Positive energy dissipation is observed at all times. All the momenta, linear and angular, are conserved for both schemes (until blow-up for the mid-point rule). We note that the continuum contributions in both cases are discretized in time using the energy-momentum conserving scheme.

note that the tangential frictional forces are always dissipative in this scheme, as proved in Section 3.3. Hence, they always imply an energy decrease. The oscillations in the energy are due to the normal contact component. To enforce the impenetrability constraint, energy is transfer back and forth to the regularization potentials, as shown in Section 3.2. The energy is not lost neither created due to this process, assuring the no-increase over the initial value and with all the energy stored in these regularization potentials fully recovered upon release. The instabilities presented by the mid-point rule in this physically dissipative setting are a consequence of the lack of control of the energy in the numerical simulation. This situation is to be contrasted with the newly proposed schemes.

## 5. Summary and Concluding Remarks

We have developed in this paper a new implicit time-stepping for frictional contact problems that inherits the a-priori stability estimates of the continuum problem. In particular, the newly proposed scheme shows unconditional positive energy dissipation in the frictional problem. The total energy in a numerical simulation is shown to be under control, and no instabilities due to an unbounded growth of the energy can occur. We say that the scheme exhibits unconditional energy stability in time. Furthermore, due to the conserving properties of the contact pressure approximation, energy stability also holds in the frictionless range. Crucial to these results is the consideration of the proper definition of the gap and slip entering the constitutive laws of contact, and a new penalty regularization of the stick/slip conditions. Furthermore, the approximation of the contact forces does not introduce any linear and angular momentum in the system, as required from physical considerations.

We have presented several representative numerical simulations showing also a good numerical accuracy of the proposed methods in the solution of both quasi-static and dynamic problems. Our experience with these methods has shown not only improved stability properties in time, as identified in the previous analyses, but also a more stable enforcement of the contact constraints when compared with standard implicit schemes. We believe that the results presented herein furnish a typical example where the a-priori knowledge of the physical properties of the mechanical system leads to the design of improved numerical methods.

## Acknowledgments

The numerical simulations presented in Section 4 were obtained with FEAP, courtesy of Prof. R.L. Taylor. Financial support for this research has been provided by the AFOSR under contract no. F49620-97-1-0196 with the University of California at Berkeley. The second author was also supported by the AFOSR under contract no. 2-DJA-826 with Stanford University. This support is gratefully acknowledged.

## References

- ARMERO, F. & PETŐCZ, E. [1996] "Formulation and Analysis of Conserving Algorithms for Dynamic Contact/Impact Problems," *Computer Methods in Applied Mechanics and Engineering*, (in press)(available as report no. UCB/SEMM-96/10, UC Berkeley).
- BATHE, K.J. & CHAUDHARY [1985] "A Solution Method for Planar and Axisymmetric Contact Problems," *Int. Journal for Numerical Methods in Engineering*, **21**, 65-88.
- BELYTSCHKO, T. & NEAL, M.O. [1991] "Contact-Impact by the Pinball Algorithm with Penalty and Lagrangian Methods," *Int. Journal for Numerical Methods in Engineering*, **31**, 547-572.
- CARPENTER, N.J.; TAYLOR, R.L. & KATONA, M.G. [1991] "Lagrange Constraints for Transient Finite Element Surface Contact," *Int. Journal for Numerical Methods in Engineering*, **32**, 103-128.
- CHEN, W.H. & YEH, J.T. [1988] "A New Finite Element Technique for Dynamic Contact Problems with Friction," *J. de Mécanique théorique et appliquée* **7** *supp.* **1**, 161-175.
- CRISFIELD, M. & SHI, J. [1994] "A Co-Rotational Element/Time-Integration Strategy for Non-Linear Dynamics," *Int. Journal for Numerical Methods in Engineering*, **37**, 1897-1913.
- GONZALEZ, O. & J.C. SIMO [1995] "Exact Energy-Momentum Conserving Algorithms for General Models in Nonlinear Elasticity," *Comp. Meth Appl. Mech. Eng.*, to appear.
- HALLQUIST, J.O.; GOUDREAU, G.L. & BENSON, D.J. [1985] "Sliding Interfaces with Contact-Impact in Large-Scale Lagrangian Computations," *Computer Methods in Applied Mechanics and Engineering*, **51**, 107-137.
- HUGHES, T.J.R.; TAYLOR, R.L.; SACKMANN, J.L; CURNIER, A. & KANOKNUKUL-AHI, W. [1976] "A Finite Element Method for a Class of Contact-Impact Problems," *Computer Methods in Applied Mechanics and Engineering*, **8**, 249-276
- KIKUCHI, N. & ODEN, J.T. [1988] *Contact Problems of Elasticity: A Study of Variational Inequalities and Finite Element Methods*, SIAM, Philadelphia
- LAURSEN, T.A. [1994] "The Convected Description in Large Deformation Frictional Contact Problems," *Int. J. Sol. Struct.*, **31**, 669-681.
- LAURSEN, T. & CHAWLA, V. [1996] "Design of Energy Conserving Algorithms for Frictionless Dynamic Contact Problems," *Int. Journal for Numerical Methods in Engineering*, in press.
- LAURSEN, T. & SIMO, J.C. [1993] "A Continuum-Based Finite Element Formulation for the Implicit Solution of Multibody, Large Deformation Frictional Contact Problems," *Int. Journal for Numerical Methods in Engineering*, **36**, 3451-3485.

- 
- LEE, K. [1994] "Numerical Solution for Dynamic Contact Problems Satisfying the Velocity and Acceleration Compatibilities on the Contact Surface," *Computational Mechanics*, **15**, 189-200.
- MUNJIZA, A.; OWEN, D.R.J. & BICANIC, J. [1995] "A Combined Finite-Discrete Element Method in Transient Dynamics of Fracturing Solids," *Eng. Comp.*, **12**, 145-174.
- ODEN, J.T. & PIRES, E.P. [1984] "Algorithms and Numerical Results for Finite Element Approximations of Contact Problems with Non-classical Friction Laws," *Computers and Structures*, **19**, 137-147.
- SIMO, J.C. & HUGHES, T.J.R. [1997] *Plasticity and Viscoplasticity, Formulation and Numerical Analysis*, Springer Verlag, preprint.
- SIMO, J.C. & TARNOW, N. [1992] "The Discrete Energy-Momentum Method. Conserving Algorithms for Nonlinear Elastodynamics," *ZAMP*, **43**, 757-793.
- TAYLOR, R.L. & PAPADOPOULOS, P. [1993] "On a Finite Element Method for Dynamic Contact/Impact Problems," *Int. Journal for Numerical Methods in Engineering*, **36**, 2123-2140.
- WRIGGERS, P.; VU VAN, T. & STEIN, E. [1990] "Finite Element Formulation of Large Deformation Impact-Contact Problems with Friction," *Computers and Structures*, **37**, 319-331.

## Appendix I. The Finite Element Implementation.

We summarize in this appendix the finite element implementation of the time-stepping algorithms presented in this paper. The discrete in time weak form (3.1) of the governing equations in a typical time step  $\{t_n, t_{n+1}\}$  leads after a finite element discretization to the following algebraic equations in terms of the nodal displacements  $\mathbf{d}_{n+1}$  and nodal velocities  $\mathbf{v}_{n+1}$  at  $t_{n+1}$  (including all the bodies in contact)

$$\left. \begin{aligned} \mathbf{R} := \mathbf{f}_{ext}^{(n+\frac{1}{2})} + \mathbf{f}_c^{(n+\frac{1}{2})} - \left[ \mathbf{f}_{int}^{(n+\frac{1}{2})} + \frac{1}{\Delta t} \mathbf{M} (\mathbf{v}_{n+1} - \mathbf{v}_n) \right] = 0, \\ \frac{1}{\Delta t} (\mathbf{d}_{n+1} - \mathbf{d}_n) = \mathbf{v}_{n+\frac{1}{2}}, \end{aligned} \right\} \quad (\text{I.1})$$

defining the (nodal) finite element residual  $\mathbf{R}$ . In (I.1),  $\mathbf{M}$  denotes the finite element mass matrix,  $\mathbf{f}_{ext}^{(n+\frac{1}{2})}$  the contributions from external loading  $\mathbf{f}_c^{(n+\frac{1}{2})}$  the contact force, and  $\mathbf{f}_{int}^{(n+\frac{1}{2})}$  the contributions from internal stresses. For example, this internal force for a isoparametric element in the mid-point discretization (3.1) reads

$$\mathbf{f}_{int}^{(n+\frac{1}{2})} = \sum_{i=1}^2 \int_{\Omega^{(i)}} \mathbf{B}_{n+\frac{1}{2}}^{(i)T} \mathbf{S}^{(i)} d\Omega^{(i)}, \quad \text{where} \quad \mathbf{B}_{n+\frac{1}{2}}^{(i)A} = \begin{bmatrix} \boldsymbol{\varphi}_{,1}^{(i)T} N_{,1}^A \\ \boldsymbol{\varphi}_{,2}^{(i)T} N_{,2}^A \\ \boldsymbol{\varphi}_{,1}^{(i)T} N_{,2}^A + \boldsymbol{\varphi}_{,2}^{(i)T} N_{,1}^A \end{bmatrix}_{n+\frac{1}{2}}, \quad (\text{I.2})$$

for each node  $A = 1, n_{node}$  with the corresponding shape function  $N^A$  ( $N_{,k}^A = k$  cartesian derivative), in a plane problem and expressed in the reference configuration. The stresses  $\mathbf{S}^{(i)}$  are given by (3.12) for the energy-conserving scheme. The rows  $\boldsymbol{\varphi}_{,k}^{(i)T}$  correspond to the columns of the deformation gradient  $\mathbf{F}^{(i)}$ .

The contact force in (I.1) is obtained in this work through the widely used master/slave logic developed in HALLQUIST et al [1985]. In this context, let  $S$  denote a typical slave node of the discretized  $\Gamma^{(1)}$  surface that comes into contact with a master segment of the discretized boundary  $\Gamma^{(2)}$  defined by nodes  $\{M1, M2, \dots\}$ . Double pass techniques avoid the prevalent role of the surface of each of the two bodies in contact; see HALLQUIST et al [1985] for details. Hence, each slave node in contact is assigned two or more master nodes defining a contact pair (or element). The simulation in Section 4 consider bilinear elements defining two-node linear master segment. Thi situation is illustrated in Figure I.1. We present below the expressions for the contact forces and their linearization for this common case only. Plane problems are considered. The general case can be obtained accordingly.

The contact force  $\mathbf{f}_c^{(n+\frac{1}{2})}$  is then expressed as

$$\mathbf{f}_c^{(n+\frac{1}{2})} = \mathbf{A}^{n_{slave}} \hat{\mathbf{f}}_{s,c}^{(n+\frac{1}{2})}, \quad \text{with} \quad \hat{\mathbf{f}}_{s,c}^{(n+\frac{1}{2})} = f_{N_s} \hat{\mathbf{G}}_{s,n+\frac{1}{2}} + f_{T_s} \hat{\mathbf{H}}_{s,n+\frac{1}{2}} \quad (\text{I.3})$$

where  $\mathbf{A}_{s=1}^{n_{slave}}$  denotes the assembly over the  $n_{slave}$  slave node/master segment pairs. The values of the normal forces  $f_N$  and  $f_T$  are obtained by integration along the slave surface  $\Gamma^{(1)}$ . As it is customary, we consider nodal quadrature rules, defining the slave node/master segments described above, leading to the so-called node-on-segment contact. In this way, we have

$$f_{N_s} = \hat{p} w_s \quad \text{and} \quad f_{T_s} = \hat{t}_T w_s, \quad (\text{I.4})$$

with the nodal pressure  $\hat{p}$  and tangential traction given by (3.16) and Table 3.2, respectively. In (I.4), we have denoted the corresponding weight of each slave node  $S$  by  $w_s$ , including the corresponding jacobian (reference length of slave segment). To simplify the implementation, one can define variable penalty parameters for each slave node, such that  $\hat{\kappa}_n := \kappa_N w_s$  and  $\hat{\kappa}_T := \kappa_T w_s$  are constant among all the slave nodes. All the arguments presented in this paper apply to this case.

In (I.3), we have used the following notation

$$\widehat{\mathbf{G}}_{n+\frac{1}{2}} = \begin{bmatrix} \boldsymbol{\nu}_{n+\frac{1}{2}} \\ -N^{M1}(\xi_s) \boldsymbol{\nu}_{s,n+\frac{1}{2}} \\ -N^{M2}(\xi_s) \boldsymbol{\nu}_{s,n+\frac{1}{2}} \end{bmatrix}, \quad \text{and} \quad \widehat{\mathbf{H}}_{s,n+\frac{1}{2}} = \frac{1}{l_s} \widehat{\mathbf{T}}_{s,n+\frac{1}{2}} - \frac{g_{s,n+\frac{1}{2}}}{l_s^2} \widehat{\mathbf{D}}_{s,n+\frac{1}{2}}, \quad (\text{I.5})$$

where

$$\widehat{\mathbf{D}}_{s,n+\frac{1}{2}} = \begin{bmatrix} \mathbf{0} \\ -N_{,\xi}^{M1}(\xi_s) \boldsymbol{\nu}_{s,n+\frac{1}{2}} \\ -N_{,\xi}^{M2}(\xi_s) \boldsymbol{\nu}_{s,n+\frac{1}{2}} \end{bmatrix}, \quad \text{and} \quad \widehat{\mathbf{T}}_{s,n+\frac{1}{2}} = \begin{bmatrix} \hat{\boldsymbol{\tau}}_{n+\frac{1}{2}} \\ -N^{M1}(\xi_s) \hat{\boldsymbol{\tau}}_{s,n+\frac{1}{2}} \\ -N^{M2}(\xi_s) \hat{\boldsymbol{\tau}}_{s,n+\frac{1}{2}} \end{bmatrix}. \quad (\text{I.6})$$

We denote by  $\hat{\boldsymbol{\tau}}_{s,n+\frac{1}{2}} = \boldsymbol{\tau}_{s,n+\frac{1}{2}}/l_s$ , the normalized tangent vector, with  $l_s = \|\boldsymbol{\tau}_{s,n+\frac{1}{2}}\|$ , the length of the contact segment at the mid-point configuration in this linear two dimensional setting. The one-dimensional shape functions  $N^{M1}$  and  $N^{M2}$  are considered in the above expressions, with

$$N^{M1}(\xi_s) = 1 - \xi_s \quad \text{and} \quad N^{M2}(\xi_s) = \xi_s, \quad (\text{I.7})$$

and consequently  $N_{,\xi}^{M1} = -N_{,\xi}^{M2} = -1$ . See Figure I.1.

With this notation, we can write the equation (3.15) defining the dynamic gap as

$$g_{s,n+1}^d = g_{s,n}^d + \widehat{\mathbf{G}}_{s,n+\frac{1}{2}}^T \left[ \hat{\mathbf{d}}_{s,n+1} - \hat{\mathbf{d}}_{s,n} \right], \quad (\text{I.8})$$

and (3.21) defining the dynamic slip as

$$\xi_{s,n+1}^d = \xi_{s,n}^d + \widehat{\mathbf{H}}_{s,n+\frac{1}{2}}^T \left[ \hat{\mathbf{d}}_{s,n+1} - \hat{\mathbf{d}}_{s,n} \right]. \quad (\text{I.9})$$



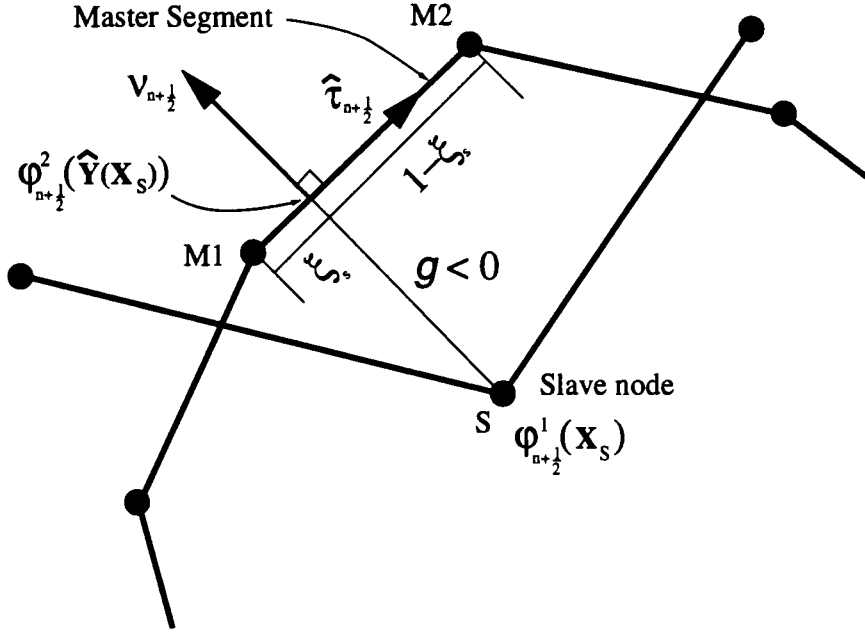


**FIGURE I.1.** Slave-node/master-segment pair for the case of linear segments in two dimensions, depicting the closest-point projection and related geometric quantities at the mid-point configuration.

Note that  $A_{\alpha\beta} \equiv l_s$  in this two dimensional case with linear master segments. Here, we have denoted

$$\hat{\mathbf{d}}_{s,n+\frac{1}{2}} = \begin{bmatrix} \mathbf{d}_{n+\frac{1}{2}}^S \\ \mathbf{d}_{n+\frac{1}{2}}^{M1} \\ \mathbf{d}_{n+\frac{1}{2}}^{M2} \end{bmatrix}, \quad (\text{I.10})$$

referring to the nodal displacements of a typical contact element (pair).

A Newton-Raphson scheme is implemented to solve the nonlinear system of equations (I.1). Hence, given the nodal values  $\{\mathbf{d}_n, \mathbf{v}_n\}$  at time  $t_n$ , we consider the consistent linearization of (I.1), leading to the algebraic system of equations

$$\left[ \frac{1}{2} \left( \mathbf{K}_{int}^{(k)} + \mathbf{K}_c^{(k)} \right) + \frac{2}{\Delta t^2} \mathbf{M} \right] \Delta \mathbf{d}_{n+1}^{(k+1)} = \mathbf{R}^{(k)}, \quad (\text{I.11})$$

in the nodal displacement and velocity increments, with the update formulas

$$\mathbf{d}_{n+1}^{(k+1)} = \mathbf{d}_{n+1}^{(k)} + \Delta \mathbf{d}_{n+1}^{(k+1)}, \quad (\text{I.12})$$

and

$$\mathbf{v}_{n+1}^{(k+1)} = \mathbf{v}_{n+1}^{(k)} + \Delta \mathbf{v}_{n+1}^{(k+1)}, \quad (\text{I.13})$$

for the values of the displacements and velocities at time  $t_{n+1}$  and iteration  $(k+1)$ . In (I.11), we have introduced the notation

$$\Delta \mathbf{f}_{int}^{(n+\frac{1}{2})} := \mathbf{K}_{int}^{(k)} \Delta \mathbf{d}_{n+\frac{1}{2}}^{(k+1)} \quad (\text{I.14})$$

with  $\Delta \mathbf{d}_{n+\frac{1}{2}}^{(k+1)} = \frac{1}{2} \Delta \mathbf{d}_{n+1}^{(k+1)}$  for the continuum contributions to the tangent stiffness, with material and geometric parts, as usual. Details are omitted. We also introduced the contact stiffness matrix

$$\Delta \mathbf{f}_c^{(n+\frac{1}{2})} := -\mathbf{K}_c^{(k)} \Delta \mathbf{d}_{n+\frac{1}{2}}^{(k+1)}, \quad (\text{I.15})$$

where

$$\mathbf{K}_c^{(k)} = \mathbf{A}_{s=1}^{n_{slave}} \widehat{\mathbf{K}}_s, \quad \text{with} \quad \Delta \widehat{\mathbf{f}}_c^{(n+\frac{1}{2})} := \widehat{\mathbf{K}}_s \Delta \widehat{\mathbf{d}}_{n+\frac{1}{2}}^{(k+1)}, \quad (\text{I.16})$$

(note the change of sign) for the contribution of the contact arrays.

The linearization of the nodal contact forces (I.3)<sub>2</sub> leads to

$$\begin{aligned} \Delta \widehat{\mathbf{f}}_{s,c}^{(n+\frac{1}{2})} = & \underbrace{\Delta f_{N_s} \widehat{\mathbf{G}}_{s,n+\frac{1}{2}}}_{\text{material normal part}} + \underbrace{f_{N_s} \Delta \widehat{\mathbf{G}}_{s,n+\frac{1}{2}}}_{\text{geometric normal part}} \\ & + \underbrace{\Delta f_{T_s} \widehat{\mathbf{H}}_{s,n+\frac{1}{2}}}_{\text{material tangential part}} + \underbrace{f_{T_s} \Delta \widehat{\mathbf{H}}_{s,n+\frac{1}{2}}}_{\text{geometric tangential part}}, \end{aligned} \quad (\text{I.17})$$

These different contributions lead to the decomposition

$$\widehat{\mathbf{K}}_s = \widehat{\mathbf{K}}_{s,N}^{mat} + \widehat{\mathbf{K}}_{s,N}^{geo} + \widehat{\mathbf{K}}_{s,T}^{mat} + \widehat{\mathbf{K}}_{s,T}^{geo}. \quad (\text{I.18})$$

The expressions for each of these parts of the contact stiffness matrix are summarized in Table I.4, with the following additional notation

$$\widehat{\mathbf{S}}_{s,n+\frac{1}{2}} = \begin{bmatrix} \mathbf{0} \\ -N_{,\xi}^{M1}(\xi_c) \widehat{\boldsymbol{\tau}}_{n+\frac{1}{2}} \\ -N_{,\xi}^{M2}(\xi_c) \widehat{\boldsymbol{\tau}}_{n+\frac{1}{2}} \end{bmatrix}, \quad (\text{I.19})$$

and the scalar factors

$$\begin{aligned} c_1 &= \frac{1}{l_s} \widehat{\mathbf{T}}_{s,n+\frac{1}{2}}^T \left( \widehat{\mathbf{d}}_{s,n+1} - \widehat{\mathbf{d}}_{s,n} \right) + \frac{g_{s,n+\frac{1}{2}}}{l_s} \boldsymbol{\nu}_{n+\frac{1}{2}}^T \left( \widehat{\boldsymbol{\tau}}_{n+1} - \widehat{\boldsymbol{\tau}}_n \right), \\ c_2 &= \boldsymbol{\nu}_{n+\frac{1}{2}}^T \left( \widehat{\boldsymbol{\tau}}_{n+1} - \widehat{\boldsymbol{\tau}}_n \right). \end{aligned} \quad (\text{I.20})$$

**TABLE I.3.** Consistent contact stiffness matrices for a linear contact pair with slave node  $S$ .

i. *Material normal stiffness:*

$$\widehat{\mathbf{K}}_{N_s}^{mat} = \mathbf{A}_{s=1}^{n_{slave}} w_s \left( \frac{U'(g_{s,n+1}^d) - \hat{p}}{g_{s,n+1}^d - g_{s,n}^d} \right) \widehat{\mathbf{G}}_{s,n+\frac{1}{2}} \otimes \left[ 2\widehat{\mathbf{G}}_{s,n+\frac{1}{2}} - c_1 \widehat{\mathbf{D}}_{s,n+\frac{1}{2}} - c_2 \widehat{\mathbf{T}}_{s,n+\frac{1}{2}} \right],$$

with the difference quotient in the first term replaced by  $U''(g_{s,n+1}^d)$  if  $g_{s,n+1}^d = g_{s,n}^d$ .

ii. *Geometric tangential stiffness:*

$$\widehat{\mathbf{K}}_{N_s}^{geo} = \mathbf{A}_{s=1}^{n_{slave}} \frac{f_{N_s}}{l_s} \left[ \widehat{\mathbf{T}}_{s,n+\frac{1}{2}} \otimes \widehat{\mathbf{D}}_{s,n+\frac{1}{2}} + \widehat{\mathbf{D}}_{s,n+\frac{1}{2}} \otimes \widehat{\mathbf{T}}_{s,n+\frac{1}{2}} + \frac{g_{s,n+\frac{1}{2}}}{l_s} \widehat{\mathbf{D}}_{s,n+\frac{1}{2}} \otimes \widehat{\mathbf{D}}_{s,n+\frac{1}{2}} \right].$$

iii. *Material tangential stiffness:* For a stick step

$$\widehat{\mathbf{K}}_{T,stick_s}^{mat} = w_s \kappa_T \vartheta \bar{M}_{\alpha\beta} \widehat{\mathbf{H}}_{s,n+\frac{1}{2}} \otimes \left[ \widehat{\mathbf{H}}_{s,n+\frac{1}{2}} + \frac{1}{f_{T_s}} \widehat{\mathbf{K}}_T^{geoT} (d_{n+1} - d_n) \right],$$

and for a slip step,

$$\begin{aligned} \widehat{\mathbf{K}}_{T,slip_s}^{mat} = & -w_s \mu \text{sign}(t_{T_s}) \left( \frac{U'(g_{s,n+1}^d) - \hat{p}}{g_{s,n+1}^d - g_{s,n}^d} \right) \widehat{\mathbf{H}}_{s,n+\frac{1}{2}} \otimes \left[ 2\widehat{\mathbf{G}}_{s,n+\frac{1}{2}} \right. \\ & \left. - c_1 \widehat{\mathbf{D}}_{s,n+\frac{1}{2}} - c_2 \widehat{\mathbf{T}}_{s,n+\frac{1}{2}} \right] \\ & - w_s \mu \hat{p} \frac{\text{sign}(t_{T_s})}{l_s} \widehat{\mathbf{H}}_{s,n+\frac{1}{2}} \otimes \widehat{\mathbf{S}}_{s,n+\frac{1}{2}}, \end{aligned}$$

with the difference quotient in the first term replaced by  $U''(g_{s,n+1}^d)$  if  $g_{s,n+1}^d = g_{s,n}^d$ .

iv. *Geometric tangential stiffness:*

$$\begin{aligned} \widehat{\mathbf{K}}_{T_s}^{geo} = & \frac{f_{T_s}}{l_s^2} \left[ 2 \left( \widehat{\mathbf{S}}_{s,n+\frac{1}{2}} \otimes \widehat{\mathbf{H}}_{s,n+\frac{1}{2}} + \widehat{\mathbf{H}}_{s,n+\frac{1}{2}} \otimes \widehat{\mathbf{S}}_{s,n+\frac{1}{2}} \right) \right. \\ & - \widehat{\mathbf{G}}_{s,n+\frac{1}{2}} \otimes \widehat{\mathbf{D}}_{s,n+\frac{1}{2}} - \widehat{\mathbf{D}}_{s,n+\frac{1}{2}} \otimes \widehat{\mathbf{G}}_{s,n+\frac{1}{2}} \\ & \left. - \widehat{\mathbf{T}}_{s,n+\frac{1}{2}} \otimes \widehat{\mathbf{S}}_{s,n+\frac{1}{2}} - \widehat{\mathbf{S}}_{s,n+\frac{1}{2}} \otimes \widehat{\mathbf{T}}_{s,n+\frac{1}{2}} \right]. \end{aligned}$$